Sensors & Diagnostics

CRITICAL REVIEW

View Article Online
View Journal

Cite this: DOI: 10.1039/d6sd00023a

Aptamer- and DNAzyme-based biosensors for pathogen detection: diagnostic strategies and clinical applications

Yunting Fan,[a] Ruiqin Jiang,[a] Hongyan Liu,[a] Wei Tian,[a] Meng Liu *[ab] and Zijie Zhang *[ab]

Pathogens that cause infectious diseases continue to pose threats to human health. The development of efficient and accurate diagnostic methods is essential for the prevention and control of pathogen infections. Functional nucleic acids (FNAs), mainly aptamers and DNAzymes, offer unique advantages for diagnostic applications. FNA-based biosensors have been widely applied in pathogen detection. This review introduces recent advances in aptamer- and DNAzyme-based biosensors for pathogen detection, with a focus on diagnostic strategies targeting diverse pathogenic targets, including genomic nucleic acids, antigens, and intact bacterial cells or viral particles. We first introduce the major classes of infectious pathogens and their health risks, followed by an analysis of their potential diagnostic targets. We then discuss aptamer- and DNAzyme-based detection strategies, including DNAzymes for detecting genomic nucleic acids, the selection of bacterium-responsive DNAzymes, and the selection and engineering of aptamers for recognizing pathogen biomarkers and intact bacterial cells or viruses. Finally, we review recent progress toward the clinical translation of aptamer- and DNAzyme-based biosensors and outline current challenges and future directions in this field.

Received 30th January 2026,
Accepted 24th March 2026

DOI: 10.1039/d6sd00023a

rsc.li/sensors

1. Introduction

Pathogens are microscopic organisms that cause diseases in humans and animals. The main types of pathogens include bacteria, viruses, fungi, mycoplasmas and protozoa. They spread through routes such as food, water, air, saliva, blood, or sexual contact.[1] These pathogens invade host cells and replicate, leading to pathological changes and clinical symptoms.[2]

Throughout history, pathogen caused-infectious diseases have led to several epidemic or pandemic events, such as the Black Death in 14th-century Europe,[3] smallpox in 15th-century America,[4] cholera pandemics in the 19th century,[5] and the influenza pandemic in the 20th century.[6] In the 21st century, emerging infectious diseases have continued to appear due to altered human activity and environmental degradation,[7] such as severe acute respiratory syndrome coronavirus (SARS-CoV, 2003),[8] swine influenza virus (SIV, 2005),[9] Middle East respiratory syndrome coronavirus (MERS-CoV, 2012),[10] and Ebola virus (EBOV, 2013).[11] The COVID-19 pandemic has caused more than 778 million infections and over 7 million deaths worldwide (data from https://covid19.who.int), making it one of the gravest global health crises of this century.[12] In addition to viruses, bacterial pathogens such as *Escherichia coli* (*E. coli*),[13] *Mycobacterium tuberculosis* (*M. tuberculosis*),[14] and *Staphylococcus aureus* (*S. aureus*),[15] which cause diseases like diarrhea, tuberculosis, and pneumonia, remain a major global threat to public health and the economy. Due to many limitations of currently available prevention and treatment methods (such as vaccines and antiviral medications), developing efficient and accurate diagnostic methods for pathogen detection is crucial.

A wide range of diagnostic targets can be exploited in pathogens, including genomes, antigens, and intact bacterial cells or viral particles. Based on these targets, many techniques for directly detecting these targets have been developed, including nucleic-acid amplification (*e.g.*, PCR)[16,17] and sequencing for genetic detection,[17–19] culture-based methods for bacterial identification,[20,21] and immunoassays for antigen detection.[22–26] Although these methods are powerful, PCR and sequencing require specialized instruments and expertise; many rapid antigen tests suffer from limited sensitivity and specificity.[27,28] In addition to these direct detection methods, indirect indicators of infection diseases, such as antibodies[29] or immune cells,[30] can also be measured for diagnostics. However, such indirect methods often fail to identify early

[a] School of Environmental Science and Technology, Dalian POCT Laboratory, Key Laboratory of Industrial Ecology and Environmental Engineering (Ministry of Education), Dalian University of Technology, Dalian, 116024, China.
E-mail: mliu@dlut.edu.cn, zhangzijie@dlut.edu.cn
[b] Central Hospital of Dalian University of Technology, Dalian, 116033, China

infections due to the time needed for the immune system to generate detectable antibodies or cells,[31] creating a diagnostic "window period". These limitations highlight the urgent need for diagnostic technologies that integrate high sensitivity and specificity with rapid, simple operation to help prevent future pandemics.

Functional nucleic acids (FNAs) are single-stranded DNA or RNA molecules with molecular recognition[32,33] or catalysis[34] functions, primarily including aptamers and DNAzymes. They are typically isolated from large random-sequence nucleic acid pools through *in vitro* selection, also known as systematic evolution of ligands by exponential enrichment (SELEX).[35] FNAs offer several advantages for diagnostic applications, including broad target recognition (from small molecules to proteins and living cells),[36–38] cost-effective and consistent chemical synthesis, and facile modification for enhanced stability and functionality.[39–41] To date, a large number of FNAs have been derived and many FNA-based biosensors have been developed for pathogen detection in clinical applications.

In the past decades, research on FNAs for pathogen diagnostics has seen tremendous development. While many reviews on various aspects of FNAs for pathogen detection have been published,[1,35,40,42–51] this review focuses on aptamer- and DNAzyme-based diagnostic strategies categorized by pathogen types and potential diagnostic targets, including nucleic acids, antigens, and intact cells or viral particles, aiming to provide practical guidance for selecting appropriate diagnostic approaches and to highlight recent advances in clinical applications. We begin by introducing the diverse types of pathogens that cause infectious diseases and analyzing their potential diagnostic components. We then discuss aptamer- and DNAzyme-based diagnostic strategies, including DNAzymes for detecting pathogen genomic nucleic acids, *in vitro* selection of bacterium-responsive DNAzymes, and the selection and engineering of aptamers for recognizing pathogen biomarkers as well as intact bacterial cells and viral particles. Next, we review recent advancements in aptamer- and DNAzyme-based biosensors for clinical pathogen detection. Finally, we discuss current challenges in the field and provide perspectives on future research directions.

2. Pathogens and potential targets for diagnostics

Infectious diseases are mainly caused by bacteria, viruses, fungi, protozoa, mycoplasmas, and prions (Fig. 1A). These pathogens exhibit distinct biological characteristics and impacts on human health. Bacteria are unicellular prokaryotes with independent metabolism. For example, *Pseudomonas aeruginosa* (*P. aeruginosa*),[52] *Salmonella typhimurium* (*S. typhimurium*),[53] and *Clostridium difficile* (*C. difficile*)[54] cause sepsis and gastroenteritis. Viruses, composed of nucleic acids (DNA or RNA) enclosed in a capsid (often with a lipid–protein envelope), lack autonomous metabolism and rely on host cells for replication.[43] Notable examples include human immunodeficiency virus (HIV),[55] human papillomavirus (HPV),[56] and poliovirus,[57] which cause AIDS and other severe diseases. In addition, fungi are eukaryotes that can trigger tissue inflammation and produce toxic metabolites (*e.g.*, aflatoxins in moldy grains)[58] that threaten food safety. Protozoa are unicellular eukaryotes, often transmitted *via* multiple hosts, and are responsible for diseases such as malaria, leishmaniasis, and trypanosomiasis.[59–61] Mycoplasmas are wall-less prokaryotes with high morphological plasticity, causing respiratory and urogenital infections.[62] Prions are misfolded proteins (PrPSc, no nucleic acids) that convert normal prion proteins (PrPC) into pathogenic forms, leading to fatal neurodegenerative disorders such as transmissible spongiform encephalopathies;[63] they are highly resistant to heat, UV, and disinfectants.[64]

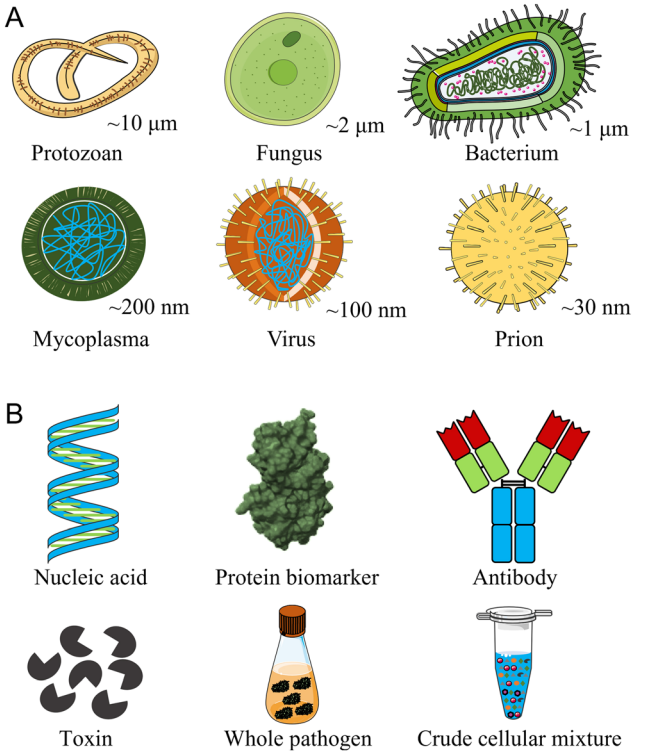

Fig. 1 (A) Types of pathogens and (B) potential targets for diagnostics.

Among these pathogens, bacteria and viruses pose the greatest threat to human health and economic burden because of their high morbidity and mortality. Current strategies to combat these pathogens include drugs, vaccines, and prevention measures. However, these approaches face challenges. For example, improper or excessive drug use can lead to resistance.[65] Frequent viral mutations reduce the efficacy of vaccines and diagnostic methods, requiring regular vaccine updates.[66] In addition, asymptomatic carriers (*e.g.*, tuberculosis, hepatitis B, and COVID-19) hinder efforts to interrupt transmission through routine screening.[19,67] To develop effective diagnostic approaches and treatments, a

thorough analysis of the potential targets of these diverse pathogens is crucial.

There are six main types of potential targets for pathogen detection, including genome nucleic acids, protein biomarkers (*e.g.*, enzymes and antigens), antibodies, toxin molecules, intact bacterial cells or virions, and crude cellular mixtures (Fig. 1B). Nucleic acids, the genetic material of pathogens, are often detected *via* polymerase chain reaction (PCR)[16,17] and sequencing techniques[17–19] to identify pathogen species and genotype variants, and assess virulence or antimicrobial resistance. Protein biomarkers, which serve as measurable indicators of specific pathogens, such as enzymes and antigens, can be detected through enzyme-linked immunosorbent assay (ELISA),[24] western blotting (WB),[25] or agglutination assays,[26] which enable rapid detection without the need for amplification. Pathogen-secreted toxins are typically analyzed by high-performance liquid chromatography (HPLC),[68] which allows precise profiling of infections in complex samples. Though effective, detection of these targets cannot distinguish intact, live pathogens from damaged or inactivated ones, often resulting in false-positive diagnostic results.[43,45]

Intact bacterial cells or viral particles are also ideal diagnostic targets. They are typically detected *via* culture-based methods combined with sequencing analysis.[20,21] But the approach is limited because not all pathogen species can be successfully cultured.[44] In addition to these targets for direct detection, host-generated antibodies after infection are also commonly used for pathogen diagnosis.[29] However, antibody detection cannot support early diagnosis due to the delay in antibody production by immune systems.[31]

Recently, instead of using a defined target for detection, crude mixtures of targets derived either from the extracellular or intracellular components of a bacterium have been used for pathogen diagnosis. This method takes advantage of small differences in the molecular compositions of complex mixtures among different bacterial species. Several DNAzymes have been successfully selected to recognize specific bacteria using this approach.[69–81] This strategy enables rapid screening of functional elements for pathogen recognition.[35] A key challenge of using crude mixtures is to identify the precise molecular targets, which requires further investigations.[35]

In conclusion, different types of targets have their own advantages and challenges for pathogen diagnosis, and selecting the appropriate target is important for accurate detection of infectious diseases. FNAs, primarily DNAzymes and aptamers, offer versatile diagnostic strategies for various pathogen targets. In the following section, we discuss FNA-based diagnostic strategies, including the use of RNA-cleaving DNAzymes (RCDs) for detecting genomic nucleic acids, bacteria-responsive DNAzymes selected using crude extracellular or intracellular mixtures, and aptamers for recognizing pathogen biomarkers or intact bacterial cells and viral particles.

3. Aptamers and DNAzymes for detection of pathogens

Nucleic acids were long considered solely as carriers of genetic information until the discovery of ribozymes (RNA catalysts) in the 1980s, which showed that nucleic acids have additional functional roles.[82] DNA and RNA share similar structures, but the stability of RNA is about one-million-fold less compared to DNA, making DNA a more promising material for practical applications.[35] In contrast to functional RNA molecules (ribozymes and riboswitches) that can be found in nature, functional DNA molecules (DNAzymes and aptamers) are isolated through *in vitro* selection using the SELEX technique.[35] To date, a large number of synthetic DNAzymes and aptamers have been developed.[35,50] They exhibit high catalytic or binding abilities, stability, ease of synthesis and modification, and low immunogenicity.[39–41] These properties make them ideal tools for pathogen recognition and the diagnosis of infectious diseases. This section introduces DNAzyme- and aptamer-based strategies for detecting diverse pathogens.

3.1. DNAzymes for detection of pathogens

3.1.1. DNAzyme basics. DNAzymes are single-stranded DNA (ssDNA) molecules with catalytic activity. The first DNAzyme was discovered with cleavage activity by Joyce's group in 1994.[34] Since then, various DNAzymes that can catalyze a wide range of reactions have been selected, such as RNA cleavage,[83] RNA ligation,[84] RNA phosphorylation,[85] DNA cleavage,[86] DNA ligation,[87] DNA phosphorylation,[88] DNA capping,[89] amide bond hydrolysis,[90] nucleopeptide bond formation,[91] and porphyrin metallase[92] as well as peroxidase activities.[93] Most of these activities depend on specific substances including metal ions, biomolecules and bacteria. Therefore, DNAzymes have been engineered as biosensors for detecting such substances.

The most widely used DNAzymes are RCDs. An RCD typically consists of two recognition arms and a catalytic core. Representative examples include the 8–17 and 10–23 DNAzymes (Fig. 2A and B), which are broadly used in pathogen RNA detection owing to their high catalytic efficiency and wide substrate compatibility.[94] RCDs commonly catalyze a transesterification reaction between the phosphodiester linkage and the adjacent 2′-hydroxyl group, producing two fragments with a 2′-3′ cyclic phosphate and a 5′-OH terminus (Fig. 2C). By rationally designing the recognition-arm sequences, RCDs can recognize and cleave RNA at defined dinucleotide junctions, such as 5′…A↓G…3′ or 5′…R↓Y…3′, where R denotes a purine base and Y a pyrimidine base.

RCDs are generated from random DNA libraries through *in vitro* selection (SELEX). A typical selection workflow includes library construction (containing 10^{14}–10^{16} random-sequenced DNA molecules), target incubation, isolation of functional sequences (a critical step), PCR amplification, and

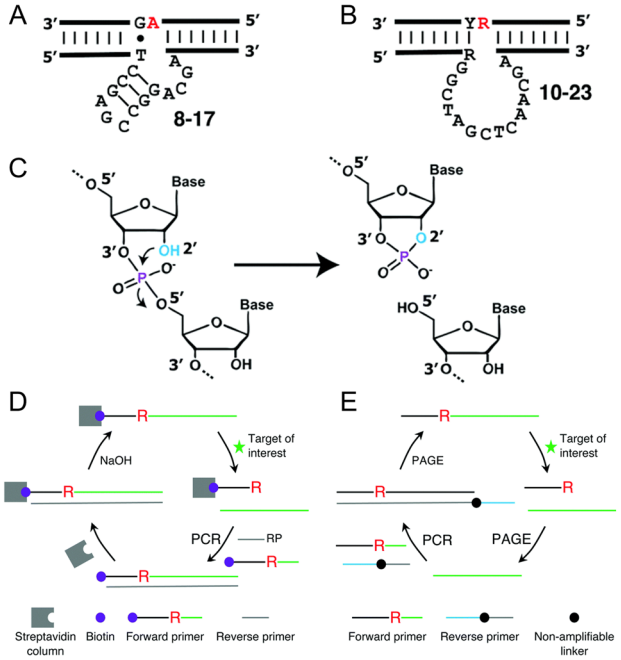

Fig. 2 Representative RNA-cleaving DNAzymes (A) 8–17 and (B) 10–23. "R" denotes a purine base and "Y" a pyrimidine base. (C) Chemical mechanism of RNA cleavage by RCDs. Reprinted with permission from ref. 94, Copyright 2017 American Chemical Society. (D) Magnetic bead (MB)-based selection strategy and (E) gel electrophoresis-based selection strategy for RCDs. Reprinted with permission from ref. 35, Copyright 2021 The Royal Society of Chemistry.

library regeneration for the next selection round (typically 7–15 cycles). Two main SELEX-based strategies are commonly employed:[35] in the magnetic bead (MB)-based method (Fig. 2D), a biotinylated library containing embedded ribonucleotide cleavage sites is produced during PCR and immobilized on streptavidin-coated magnetic beads. Unmodified strands are removed with NaOH before target incubation. Functional sequences then cleave the substrate strands, dissociate from the beads, and are collected, amplified, and advanced to the next round. In the denaturing polyacrylamide gel electrophoresis (dPAGE) method (Fig. 2E), DNA strands containing cleavage sites are first separated by electrophoresis. After target incubation, functional sequences self-cleave to generate shorter fragments, which are recovered through a second electrophoresis step, amplified, and used for subsequent rounds.

RCDs can act on diverse RNA substrates, including chimeric substrates with a single RNA linkage, all-RNA substrates, and fluorogenic substrates, in which the RNA linkage is flanked by deoxyribothymidines labeled with a fluorophore (F) and a quencher (Q). All-RNA substrates allow selection of RCDs that cleave biologically relevant RNAs, chimeric substrates enable precise control over the cleavage site, and fluorogenic substrates are particularly suited for developing RCDs for biosensing applications.[94]

3.1.2. DNAzymes for detection of genomic nucleic acids of pathogens. Existing technologies for detecting the genomic nucleic acids (DNA or RNA) of pathogens still face challenges. For example, quantitative reverse-transcription real-time PCR (qRT-PCR) is widely used to detect viral RNA of SARS-CoV-2. However, PCR-based methods require a long testing period (usually more than 24 h) and rely on specialized instrumentation and controlled laboratory conditions.[16,17] Other nucleic acid amplification techniques, including recombinase polymerase amplification (RPA) and loop-mediated isothermal amplification (LAMP), offer shorter detection times but show limitations in sensitivity and specificity.[95–97] CRISPR-based systems detect pathogen nucleic acids by using guide RNAs to bind complementary sequences, yet their applicability is restricted to regions adjacent to protospacer adjacent motifs (PAMs), limiting target selection.[97,98] In contrast, RCDs enable site-specific RNA cleavage and provide an effective strategy for detecting pathogen genomic nucleic acids. Numerous studies have developed RCD-based detection platforms for pathogen diagnosis.[97,99–101]

Recently, Chaput's group[99] developed the REVEALR system based on the X10–23 XNAzyme, using SARS-CoV-2 as the detection target. The prefix "X" in X10–23 stands for xeno nucleic acid (XNA), indicating that the canonical 10–23 DNAzyme has been modified with non-natural nucleic acids (*e.g.*, ANA, TNA, and GNA) to enhance its resistance to nuclease degradation. In this platform, the target RNA is initially pre-amplified through RT-RPA, after which T7 RNA polymerase produces trigger sequences that promote the assembly of X10–23 XNAzymes capable of specifically cleaving a fluorescent reporter RNA. The resulting signal can be measured by either fluorescence detection or a paper-based lateral flow assay. The system achieves a limit of detection (LOD) of ≤20 aM (~10 copies μL^{-1}) with a total assay time within 1 h. When applied to RNA extracted from nasopharyngeal swabs of 10 PCR-positive and 2 PCR-negative patients, it demonstrated 100% accuracy without cross-reactivity.

To enable viral variant genotyping, they further optimized REVEALR into a competitive binding detection platform.[97] By incorporating locked nucleic acids (LNAs) to enhance discrimination of single-base mismatches, the system can precisely distinguish SARS-CoV-2 variants based on characteristic single-nucleotide mutation sites. Using 34 nasopharyngeal swab samples (31 SARS-CoV-2-positive and 3 negative) for clinical validation, the platform achieved 100% genotyping accuracy, successfully identifying the wild-type strain and major variants, including Alpha, Gamma, Delta, and Omicron, demonstrating its potential for variant discrimination.

Li's group developed an approach for directly detecting large-genome RNAs of viruses.[100] Using SARS-CoV-2 RNA as a model, a strategy coupling 10–23 DNAzyme-mediated RNA cleavage with rolling circle amplification (RCA) was established (Fig. 3A). Through combined viral RNA secondary structure prediction and experimental validation, 28 variants of 10–23 DNAzymes capable of cleaving viral RNA were

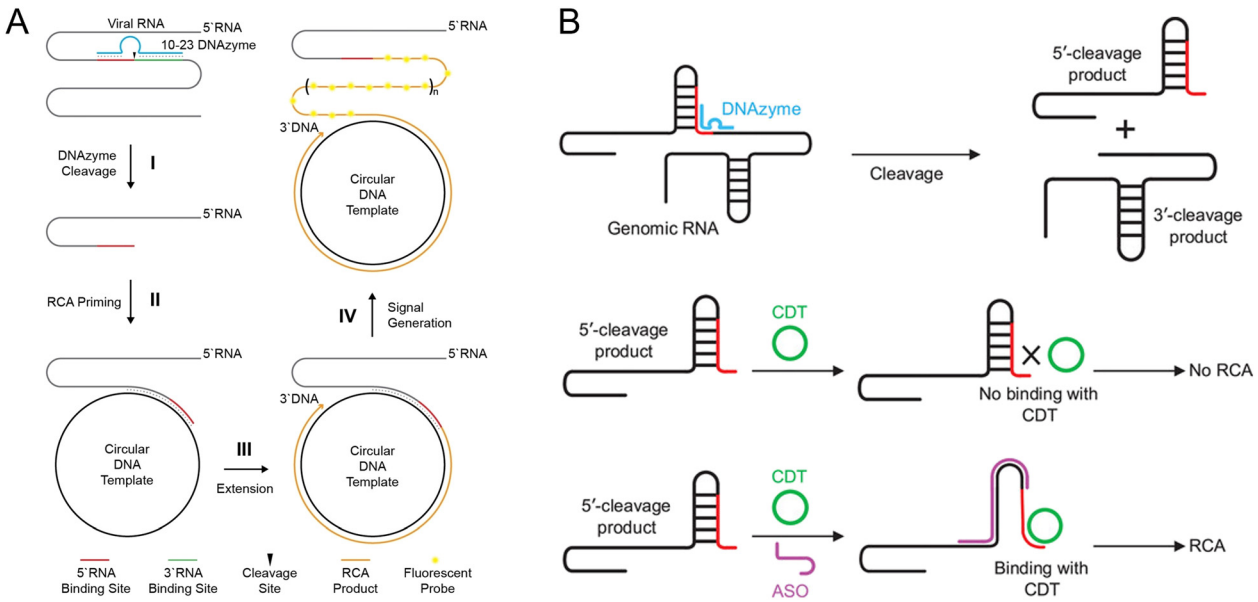

Fig. 3 (A) Schematic of 10–23 DNAzyme-mediated rolling circle amplification (RCA) for detecting SARS-CoV-2 genomic RNA. Reprinted with permission from ref. 100. Copyright 2023 Wiley-VCH Verlag GmbH & Co. KGaA, Weinheim. (B) Schematic of antisense oligonucleotide (ASO)-assisted RCA for detecting structured genomic RNA. Reprinted with permission from ref. 101. Copyright 2025 Wiley-VCH Verlag GmbH & Co. KGaA, Weinheim.

identified from 230 candidates, including one exhibiting >60% cleavage efficiency, while all variants showed efficiencies exceeding 20%. These DNAzymes specifically cleave viral RNA to generate fragments with well-defined 3′ termini, which subsequently serve as primers for circular DNA templates, initiating RCA catalyzed by ϕ29 DNA polymerase. To further enhance sensitivity, a quasi-exponential RCA strategy was implemented by incorporating a secondary primer (P2), lowering the LOD to 500 aM. Evaluation using 29 patient saliva samples, including 14 RT-PCR-confirmed SARS-CoV-2-positive and 15 negative samples across multiple variants, demonstrated a clinical sensitivity of 86% with 100% specificity. The system also eliminated the need for reverse transcription and completed detection within 2.5 h.

DNAzymes combined with RCA provide a powerful approach for detecting pathogen RNAs. However, a limitation is that the resulting RNA fragments by DNAzyme cleavage often retain secondary or tertiary structures, which hinder circular template (CDT) binding, limiting RCA efficiency. To overcome this problem, the research group further developed antisense oligonucleotide-assisted RCA (ASO-RCA),[101] a strategy that uses short upstream antisense oligonucleotides (ASOs) to remodel the RNA structure and expose CDT-binding sites (Fig. 3B). Using five DNAzyme-CDT systems targeting distinct regions of the virus genome, ASO inclusion was found to improve CDT hybridization and increase RCA output by up to 70-fold. This enhancement was observed in both linear and quasi-exponential RCA formats and remained effective in 50% pooled saliva. Applied to clinical saliva samples, ASO-assisted RCA substantially improved diagnostic performance, achieving 100% sensitivity and 97.5–100% accuracy across multiple systems. Together, these studies demonstrate that DNAzyme-based strategies can efficiently detect pathogens through highly specific cleavage activity. Coupling DNAzymes with RCA establishes a simple, robust, and clinically relevant platform for enhancing nucleic acid detection of structured RNA targets in pathogens.

3.1.3. *In vitro* selection of bacterium-responsive DNAzymes. DNAzymes were initially identified as primarily responsive to metal ions, such as Pb^{2+}, Zn^{2+}, Mg^{2+}, Cu^{2+}, and Ca^{2+}.[35,44,102] Recent studies have shown that DNAzymes can also interact with clinically relevant targets, including bacteria,[69–81] cancer cells,[103] and small metabolites.[104,105]

Li's group pioneered a strategy for selecting bacteria-responsive RNA-cleaving fluorescent DNAzymes (RFDs) using crude extracellular (CEM) or intracellular mixtures (CIM).[69] In the RFD constructs, the DNAzyme flanking a single ribonucleotide is labeled with a fluorophore (F) and a quencher (Q). Upon activation by the target bacterium, the RFD cleaves its substrate, separating F and Q and generating a fluorescent signal (Fig. 4A).[45] The resulting fluorescence provides a convenient and sensitive readout, facilitating rapid bacterial detection and development of DNAzyme-based biosensors.

This approach exploits compositional differences among bacterial species through alternating positive and counter selection. Instead of relying on a defined molecular target, crude mixtures from specific bacteria serve as triggers to induce cleavage of candidate RFDs, allowing the identification of DNAzymes that respond to unique cellular components of a pathogen. High specificity could be achieved *via* stringent alternating selection steps: the CEM or CIM of the target bacterium is used for positive selection,

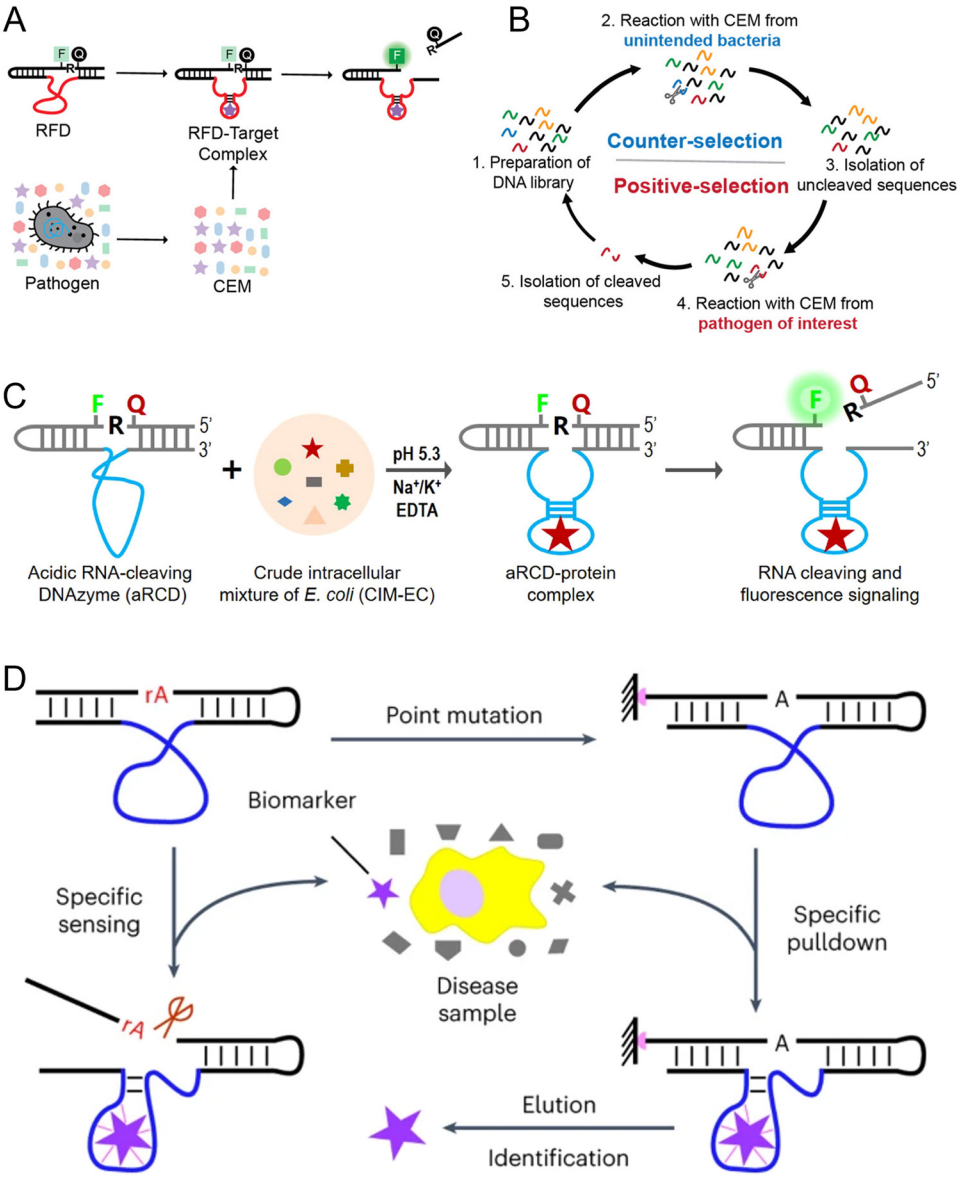

Fig. 4 (A) Design of RFDs that generate fluorescent signals in the presence of the crude extracellular mixture (CEM) of the target bacterium. F, fluorescein-dT; Q, dabcyl-dT. (B) Isolation of RFDs specific to the target bacterium using a combined positive- and counter-selection strategy. Reprinted with permission from ref. 45. Copyright 2021 American Chemical Society. (C) Selection of acidic DNAzymes for the detection of *E. coli*. Reprinted with permission from ref. 80. Copyright 2023 American Chemical Society. (D) DNAzyme-based MORAC technique for capturing potential biomarkers from complex and unknown biological systems. Reprinted with permission from ref. 103. Copyright 2024 Springer Nature.

while those from non-target bacteria are used for counter selection (Fig. 4B). In each cycle, the DNA library undergoes counter selection to remove cleaved sequences, followed by positive selection, where cleaved fragments are recovered, amplified, and used in subsequent rounds—progressively enriching RFDs specific to the target species.[45]

Based on this strategy, several bacterial-responsive RFDs have been developed, including *Legionella pneumophila* (*L. pneumophila*),[73] *S. aureus*,[74] *Fusobacterium nucleatum* (*F. nucleatum*).[75] *C. difficile*,[70,76] and *S. typhimurium*.[78] The detailed performance of these RFD-based sensing systems for bacterial detection is summarized in Table 1. These methods enable sensitive detection of target bacteria, demonstrating the high efficiency of the identified RFDs. In addition, these RFDs exhibited strong specificity, enabling discrimination among different bacterial species.

RNA is inherently unstable and readily degraded by ubiquitous RNases, which require divalent metal ions and function optimally at neutral pH. Accordingly, selecting RCDs under acidic and metal-depleted conditions can yield chemically more stable variants, thus extending their utility in unconventional environments. To this end, our group developed a divalent ion-independent, acid-responsive RNA-cleaving DNAzyme (aRCD) selection strategy for bacterial detection

Table 1 Representative DNAzymes and DNAzyme-based biosensors for pathogen detection

Pathogen	DNAzyme	k_{obs}	Sensor types	Assay time	LOD	Test sample	Ref
L. pneumophila	LP1F3′	0.125 min^{-1}	Optical	72 h	10 CFU mL^{-1}	Cooling tower water	73
S. aureus	RFD-SA6/RFD-SA6T1	—	Optical (fluorescence/colorimetric)	60 min/30 min	10^2 CFU mL^{-1}/10^5 CFU mL^{-1}	Nasal mucus	74
F. nucleatum	RFD-FN1	0.38 h^{-1}	Optical	36 h	1 CFU mL^{-1}	Human saliva/human stool	75
C. difficile	RFD-CD1	—	Optical	30 min	10^2 CFU mL^{-1}	—	76
S. typhimurium	SSR1-T4	8 min^{-1}	Optical (fluorescence/colorimetric)	1 h/1 h	3.2×10^3 CFU mL^{-1}/ 6.4×10^3 CFU g^{-1}	Ground beef/chicken/milk/eggs	78
E. coli	aRCD-EC1SF5′	1.18 min^{-1}	Optical	50 min	10^4 CFU mL^{-1}	Clinical urine samples	80
B. cocovenenans	RFD-BC1T1	0.01 min^{-1}	Optical	2 h	1 CFU	*Tremella fuciformis*	81

(Fig. 4C).[80] We selected an acidic RCD, aRCD-EC1, which is specific for *E. coli*. aRCD-EC1 only requires monovalent metal ions to cleave a fluorogenic chimeric DNA/RNA substrate. This minimizes undesired RNA degradation. Moreover, the acidic environment further stabilizes RNA phosphodiester bonds. The acidic RCD exhibited a rate constant (k_{obs}) of 1.18 min^{-1}, the fastest reported among bacteria-responsive RCDs. For clinical applications, the acidic RCD accurately diagnosed all 40 patient urine samples with 100% sensitivity and specificity. In addition, using this strategy, we further isolated another acidic RCD responsive to *Burkholderia gladioli* pv. *Cocovenenans* (*B. cocovenenans*), a pathogen associated with fatal food poisoning.[81] This RCD showed maximal activity at pH 5.0. The aRCDs were further applied in a droplet biosensing platform that can detect *B. cocovenenans* at single-cell resolution. These studies demonstrate the practical value of acidic RCDs for bacterial detection.

While using the CEM or CIM as selection targets offers certain advantages, their complex molecular composition makes it difficult to identify specific pathogen targets. Recently, Gu's group developed a DNAzyme-based molecular recognition and capture (MORAC) technology for complex systems with unknown molecular components (Fig. 4D).[103] Using SELEX, they screened DNAzymes that specifically recognize unknown molecules within biological mixtures. The RNA-cleaving activity of the DNAzymes allows highly sensitive detection of disease biomarkers and viral antigens. Interestingly, a single RNA-to-DNA point mutation abolishes catalytic activity but preserves target recognition. This converts the DNAzymes into pure affinity probes for target capture. Using MORAC, the researchers identified a low-abundance apolipoprotein L6 (APOL6) biomarker from the CEM of breast cancer cells and seryl-tRNA synthetase 1 (SARS1) from lysates of colorectal precancerous polyps. The clinical relevance of these biomarkers was confirmed, demonstrating the method's utility for discovering rare targets in complex biological samples.

3.2. Aptamers for detection of pathogens

3.2.1. Aptamer basics. Aptamers are single-stranded DNA or RNA molecules obtained through *in vitro* selection, with specific binding ability to a target molecule.[32,33] Based on Watson–Crick base pairing principles, they can fold into various secondary structures such as stems, loops, bulges, hairpins, pseudoknots, and G-quadruplexes.[106] These secondary structures further fold into unique tertiary conformations. This process is driven by intramolecular nucleotide interactions and intermolecular interactions with target molecules, including hydrogen bonding, van der Waals forces, electrostatic interactions, hydrophobic effects, base π–π stacking, and shape complementarity.[107,108] These conformations are key to high-affinity and highly specific target recognition.[44,109]

To date, thousands of synthetic DNA or RNA aptamers and nearly 40 classes of natural RNA aptamers have been discovered. Their targets span a wide range of molecules, including metal ions,[110] small molecules,[111–113] glycolipids,[114,115] proteins,[37,115–119] viruses,[120–125] cells,[126–128] bacteria,[129–137] microplastics,[138,139] and tissues.[140,141] Aptamer screening relies on SELEX technology. Specific selection strategies are developed to different targets. For example, Capture-SELEX is used for small-molecule targets,[36,111–113] MB-SELEX for protein targets,[37,117–119] and Cell-SELEX for intact live cell targets.[41,126–128] These methods have been comprehensively reviewed,[39,41,44,50,51] and will not be discussed further here. Conclusively, rational design of target-specific screening strategies is key to obtaining aptamers with high affinity and specificity.

Currently, many aptamers have been isolated for targeting various pathogens, including viruses such as HCV,[142] HPV,[143] and ZIKV,[144] as well as bacteria such as *S. aureus*,[129,130] *E. coli*,[131] and *S. typhimurium*.[132] These aptamers recognize pathogen biomarkers or intact pathogens, making them effective recognition elements for pathogen biosensors. However, pathogens are often highly mutable (*e.g.*, viruses and drug-resistant bacteria), present at low concentrations, and difficult to detect. As a result, screening aptamers with high performance remains challenging. This section will focus on aptamer selection strategies that address the pathogen mutation issue. We will also summarize aptamer screening and multivalent engineering methods developed for detecting different types of pathogen targets.

3.2.2. Aptamers for detection of mutating viruses. Viruses frequently undergo mutations, which directly reduce the effectiveness of existing diagnostic tools (*e.g.*, traditional

antibody- and aptamer-based detection) and therapies (*e.g.*, strain-specific antibody blockers).[145–147] Failure to address emerging variants can perpetuate threats to human health, overburden public health systems and cause recurrent outbreaks.[97,148]

To address this challenge, selection strategies have been developed to isolate aptamers capable of recognizing mutated viral variants with universally high affinity. Li's group developed a "universal aptamer" strategy for detecting multiple SARS-CoV-2 spike (S) protein variants, including Alpha, Beta, and Omicron (Fig. 5A).[117] Using a wild-type S protein-targeting aptamer library, they performed parallel SELEX to simultaneously enrich sequences binding five variant S proteins, yielding the universal aptamer MSA52. MSA52 recognizes eight S protein variants, with K_d: 2.8–10.2 nM for variants and 18.4–49.0 pM for pseudoviruses. This discovery demonstrates that aptamers with high affinity toward multiple variants of a single protein, including emerging forms, can be generated, making them well suited for molecular recognition of rapidly evolving targets such as SARS-CoV-2.

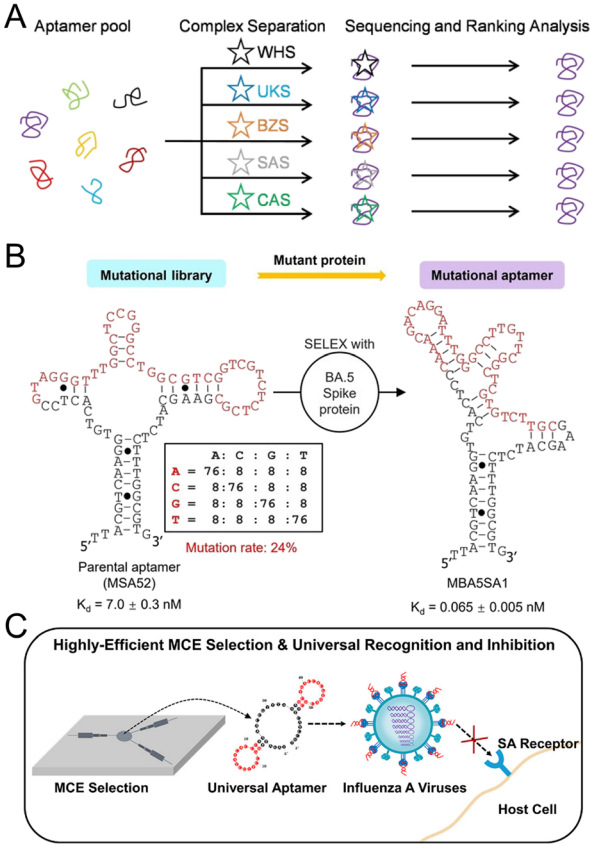

Fig. 5 (A) Schematic illustration of the selection of universal aptamer MSA52 for recognizing variant spike (S) proteins of SARS-CoV-2. Reprinted with permission from ref. 117. Copyright 2022 Wiley-VCH Verlag GmbH & Co. KGaA, Weinheim. (B) Design of a mutant library based on the MSA52 sequence for selecting new aptamers to detect mutated viral variants. Reprinted with permission from ref. 119. Copyright 2025 Wiley-VCH Verlag GmbH & Co. KGaA, Weinheim. (C) A universal aptamer for recognizing influenza A subtype viruses. Reprinted with permission from ref. 118. Copyright 2024 American Chemical Society.

As SARS-CoV-2 continues to evolve, Omicron subtypes exhibit more extensive S protein mutations, demanding even higher aptamer affinity and specificity. To address this issue, the group proposed a "fighting mutations with mutations" strategy (Fig. 5B).[119] Using MSA52 as a template, they built a partially randomized mutant library and conducted 12 SELEX rounds, generating the high-affinity aptamer MBA5SA1. MBA5SA1 has a K_d of 0.065 nM for BA.5 S protein (over 100-fold higher than MSA52) and recognizes 6 Omicron subtypes, and its truncated form (MBA5SA1-T12) shows further improved affinity (K_d: 0.043 nM). An enzyme-linked aptamer binding assay (ELABA) based on MBA5SA1 was used to test 83 saliva samples, achieving 86.5% sensitivity and 100% specificity for Omicron, demonstrating its diagnostic efficacy.

This work provides a compelling case study for identifying high-affinity aptamers targeting rapidly mutating viral proteins using a partially randomized pool derived from an existing aptamer originally selected against the parental protein. Moreover, selection from a mutagenized pool built on an aptamer with a defined secondary structure simplifies and accelerates post-SELEX sequence and structural characterization, as offspring aptamers are expected to retain conserved nucleotides and structural motifs essential for function.

Besides SARS-CoV-2, Zhang's group recently proposed a "multichannel enrichment (MCE) magnetism-controlled microfluidic SELEX" strategy targeting the diverse and mutable hemagglutinin (HA) subtypes of influenza A viruses (IAVs) (Fig. 5C).[118] HA proteins from three IAV subtypes (H5N1, H7N9, and H9N2) were immobilized on magnetic nanospheres to construct a multichannel target array, enabling enrichment of sequences binding multiple HA subtypes from a random library. After three screening rounds, the universal aptamer UHA-2 was obtained, showing broad binding affinities with K_d values of 1.5 nM for H5N1 HA, 3.7 nM for H7N9 HA, and 10.1 nM for H9N2 HA. In addition to its diagnostic potential for diverse IAV subtypes, UHA-2 broadly neutralizes five IAV subtypes (H5N1, H7N9, H9N2, H1N1, and H3N2), significantly inhibiting viral hemagglutination. In MDCK cells, UHA-2 increased survival of infected cells by up to 63%, approaching 90% survival at 1000 nM. This study not only reports a universal aptamer with broad inhibitory activity against multiple IAVs but also establishes an efficient strategy for developing universal antiviral inhibitors.

3.2.3. Aptamer engineering for high-affinity detection of pathogen biomarkers. High-affinity aptamers can be generated by engineering dimeric or multimeric constructs through the linkage of two or more monomeric aptamers. This strategy exploits multivalent interactions to enhance binding avidity and target occupancy. For example, Mayer's group combined two thrombin-binding aptamers into a

dimeric construct, achieving an approximately 30-fold improvement in affinity.[149] Similarly, Soh's group developed a bivalent aptamer through a selection-based strategy,[150] demonstrating the feasibility of rational multivalency in aptamer design.

Pathogens typically contain multiple copies of specific biomarkers, making them particularly suitable for multivalent recognition. For instance, SARS-CoV-2 virions display ~30 S proteins per particle and more than hundreds of nucleocapsid (N) proteins,[151] while influenza viruses express approximately 500 hemagglutinin (HA) proteins and 100 neuraminidase (NA) proteins,[152] and noroviruses present about 90 capsid proteins per virion.[153] Such multivalent components render dimeric and multimeric aptamers highly promising for pathogen detection. Moreover, aptamers generally target exposed and readily accessible pathogen surface biomarkers, such as envelope proteins, membrane proteins, and S proteins, which are ideal candidates for virus detection without requiring complex sample processing.[43]

Li's group targeted the SARS-CoV-2 S protein using a pre-structured DNA library combined with SELEX technology.[37] Through a hybrid selection strategy involving magnetic bead separation in the first three rounds and an electrophoretic mobility shift assay (EMSA) in the subsequent ten rounds, over 100 candidate aptamers were obtained after 13 rounds of enrichment. Among them, MSA1 (K_d = 1.8 nM) and MSA5 (K_d = 2.7 nM) exhibited the highest affinities, both featuring a predesigned hairpin structure.

To further enhance affinity toward the S protein and evaluate clinical applicability, the group developed heterodimeric aptamers.[154] Based on the truncated high-affinity monomers MSA1T and MSA5T, heterodimeric aptamers were constructed using a 30-thymidine linker (Fig. 6A). DSA1N5 displayed a K_d of 120 pM for the wild-type homotrimeric S protein, representing 99-fold and 28-fold affinity improvements compared to MSA1T and MSA5T, respectively. In addition, DSA1N5 recognized the S proteins of the Alpha and Delta variants with K_d values of 290 pM and 480 pM, respectively. In clinical detection, including saliva and wastewater samples, the dimeric aptamer achieved 80.5% sensitivity and 100% specificity, with an LOD of ≤1 copy per mL in wastewater, showing its strong diagnostic potential.

To overcome the limitation that monomeric aptamers bind only a single subunit of the S protein, the researchers further designed a homotrimeric aptamer with a threefold symmetric branched structure.[155] As illustrated in Fig. 6B, three MSA52 monomers were assembled into a symmetric trimeric construct (TMSA52) using a "trebler" scaffold, enabling precise spatial matching with the trimeric architecture of the SARS-CoV-2 S protein and achieving a "three-to-three" symmetric recognition mode. Experimental results demonstrated that TMSA52 binds S protein-expressing pseudoviruses with femtomolar-level affinity. The K_d values of TMSA52 for the S proteins of eight SARS-CoV-2 variants ranged from 8.8 to 23.7 pM, representing an approximately

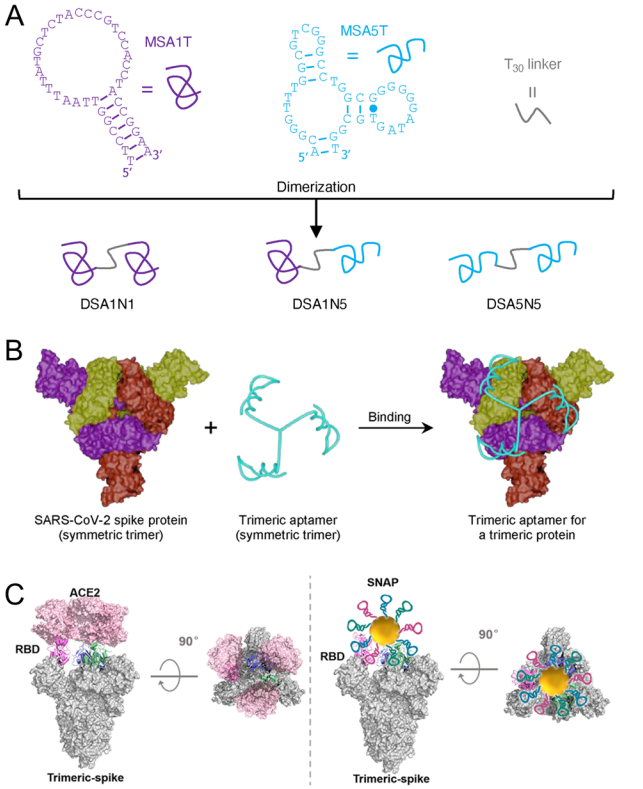

Fig. 6 (A) The secondary structures of aptamers MSA1T and MSA5T, and constructed dimeric aptamers DSA1N1, DSA1N5 and DSA5N5 for detecting the S proteins of SARS-CoV-2. Reprinted with permission from ref. 154. Copyright 2021 Wiley-VCH Verlag GmbH & Co. KGaA, Weinheim. (B) Recognition of the symmetric homotrimeric aptamer TMSA52 binding with the symmetric homotrimeric spike (S) protein of SARS-CoV-2. Reprinted with permission from ref. 155. Copyright 2022 American Chemical Society. (C) Mechanism of the spherical neutralizing aptamer (SNAP) inhibiting viral infection and suppressing mutational escape. Reprinted with permission from ref. 156. Copyright 2021 American Chemical Society.

two-order-of-magnitude enhancement in affinity relative to the monomeric aptamer. When detecting viruses in saliva, the trimeric aptamer exhibited an LOD of 6.3×10^3–1.0×10^4 copies per mL. In clinical evaluation using 110 saliva samples (50 positive and 60 negative), the sensor achieved a sensitivity of 84.0% and a specificity of 98.3%, and effectively recognized multiple variants, including wild-type, Alpha, Delta, and Omicron strains.

Besides dimeric and trimeric assemblies, aptamers can also be integrated with nanomaterials to construct higher-order multimeric systems with enhanced functionality. For example, Yang's group[156] developed a multivalent aptamer–gold nanoparticle strategy termed spherical neutralizing aptamer–gold nanoparticles (SNAP), which blocks the interaction between the SARS-CoV-2 S protein receptor binding domain (RBD) and host angiotensin-converting enzyme 2 (ACE2) (Fig. 6C). In this approach, multiple neutralizing DNA aptamers with different sequences were densely assembled on the surface of 5 nm gold nanoparticles, forming a nanocomposite that enables

synergistic multivalent and multisite blockade. The nanoparticle size closely matches the spacing between RBDs on the S protein, ensuring simultaneous and efficient binding to multiple RBD sites. SNAP exhibited an ultrahigh affinity toward RBDs (K_d = 3.90 pM). Compared with free aptamers, nanoparticle assembly effectively mitigated nuclease-mediated degradation and enhanced recognition stability in complex environments.

Multimeric aptamer strategies have also been extended beyond viruses. For instance, Xu's group[157] developed a dual-functional aptamer targeting *S. typhimurium* and binding to cinnamaldehyde (CA) through sequence truncation. Specifically, an aptamer recognizing *S. typhimurium* flagellin was truncated to retain core binding sequences (*e.g.*, the critical 5′-CA base pair), yielding a high-affinity bivalent aptamer T23-2 (K_d = 52.42 nM). Meanwhile, a CA-specific aptamer was truncated to enhance binding affinity, resulting in CA24 (K_d = 1.800 μM). These two functional aptamers (T23-2 and CA24) were further conjugated to generate a dual-functional tandem aptamer CAB-3 T. This dual-functional integration strategy significantly improved target binding and drug loading capacity: CAB-3 T exhibited a K_d of ~48.66 nM for *S. typhimurium* and a K_d of 0.4348 μM for CA, enabling precise targeting of the pathogen and stable loading of the antibacterial agent simultaneously.

In summary, dimeric and multimeric aptamer strategies markedly enhance affinity and cooperative recognition toward pathogens. Aptamer engineering not only provides powerful molecular tools for highly sensitive and specific detection of low-abundance pathogens but also accelerates the translation of nucleic acid recognition elements from fundamental research to practical applications. These studies highlight the design flexibility and engineering advantages of aptamers in addressing complex detection challenges, offering high-performance recognition elements for next-generation biosensors.

3.2.4. Aptamers for detecting intact pathogens. SELEX technology can directly target intact pathogens, such as viruses, bacteria, and fungi, without requiring prior isolation or purification of individual biomarkers. The advantage of this strategy lies in preserving the native conformation and surface molecular characteristics of pathogens, allowing diverse biomolecules on the pathogen surface to interact with aptamers.[44] The selection conditions for intact pathogens closely mimic molecular interactions in physiological environments; consequently, the resulting aptamers exhibit stronger translational potential in real-sample detection and better align with practical diagnostic needs.[43] Representative aptamers targeting intact pathogens are summarized in Table 2.

For bacterial targets, Cell-SELEX is currently the mainstream selection strategy. Compared with other SELEX derivatives, it offers simple operation and eliminates the need for immobilization of either bacterial targets or nucleic acid libraries, as centrifugation alone enables efficient separation of "active sequence–bacteria complexes" from unbound sequences. To date, aptamers and corresponding biosensors have been successfully developed for *S. aureus*,[129,130] *E. coli*,[131] *S. typhimurium*,[132] *Haemophilus influenzae* (*H. influenzae*) type b,[133] *Streptococcus pneumoniae* (*S. pneumoniae*),[134] *Vibrio vulnificus* (*V. vulnificus*),[135]

Table 2 Representative aptamers and aptamer-based biosensors for detecting intact pathogens

Type	Pathogen	Aptamer	K_d	Sensor types	Assay time	LOD	Test sample	Ref.
Bacteria	*S. aureus*	RAB35	3 nM	Optics	2 h	10^2 CFU mL^{-1}	Milk	129
	S. aureus	SA81	14.47 nM	Electrochemistry	2 h	414 CFU mL^{-1}	Tap water	130
	E. coli	Ec3(31)	225 nM	Optics/electrochemistry	1 h	5 CFU mL^{-1}/2 × 10^4 CFU mL^{-1}	—	131
	S. typhimurium	ST2P	6.33 nM	Optics	40 min	25 CFU mL^{-1}	—	132
	H. influenzae	63	28.4 pM	Optics	45 min	60 CFU mL^{-1}	Patient's cerebrospinal fluid	133
	S. pneumoniae	Lyd-3	661.8 nM	Optics	30 min	15 CFU mL^{-1}	—	134
	V. vulnificus	Vapt2	26.8 nM	Optics	60 min	8 CFU mL^{-1}	—	135
	A. salmonicida	A.s-2	32 nM	Dual-optical	2 h/35 min	1.9 × 10^2 CFU mL^{-1}/2.2 × 10^2 CFU mL^{-1}	Zebrafish	136
	B. bifidum	CCFM641-5	10.69 nM	Optics	45 min	10^4 CFU mL^{-1}	—	137
Viruses	HuNoV	SMV-21	101 nM	Optics	2 h	10 RNA copies per sample	Lettuce	120
	MNV	AG3	240 fM	Electrochemistry	1 h	180 virus particles	Meat juice	121
	MDPV	Apt-10	467 nM	Optics	1 h	1.5 EID_{50}	Duck embryo allantoic fluid	122
	HAdV	HAdV-Seq4	0.9 nM	Electrochemistry	30 min	1 PFU mL^{-1}	Tap water Wastewater	123
	SARS-CoV-2 pseudotyped virus	SARS2-AR10	79 nM	Electrochemistry	2 h	1 × 10^4 copies per mL	Saliva	123
	IBV	Apt_IBV02	58.2 nM	Optics	2.5 h	1.2 EID_{50} mL^{-1}	Tracheal/cloacal/lung/kidney	124
	AIV H5Nx	IF10/IF22	10^4 EID_{50} mL^{-1}/2 × 10^4 EID_{50} mL^{-1}	Optics	30 min	200 EID_{50} mL^{-1}	Feces	125

Aeromonas salmonicida (*A. salmonicida*),[136] and *Bifidobacterium bifidum* (*B. bifidum*).[137]

In contrast to bacteria, viruses operate at the nanoscale and are far smaller than micrometer-scale bacteria and cells, making direct centrifugation-based separation of "active sequence–virus complexes" from unbound sequences challenging. Consequently, auxiliary carriers or separation strategies are required. For example, in selecting aptamers against human noroviruses (HuNoVs), magnetic bead-based SELEX (MB-SELEX) is employed, with viruses immobilized on magnetic beads to enable rapid separation.[120] For murine norovirus (MNV), filter membrane-based SELEX (FM-SELEX) is used, leveraging molecular weight cutoff properties to retain complexes while allowing free sequences to pass through.[121] For avian influenza viruses (AIV H5Nx), graphene oxide-based SELEX (GO-SELEX) is applied, as graphene oxide selectively adsorbs free nucleic acids, thereby facilitating enrichment of active sequences.[125] To date, aptamer-based biosensors have been successfully developed for Muscovy duck parvovirus (MDPV),[122] human adenovirus (HAdV),[123] SARS-CoV-2,[123] and infectious bronchitis virus (IBV)[124] (Table 2).

4. Aptamer- and DNAzyme-based biosensors for infectious pathogen diagnosis

A biosensor is an analytical tool that integrates a biorecognition element (*e.g.*, enzymes, antibodies, DNAzymes, and aptamers) with a signal transducer. It converts specific biomolecular interactions (such as catalysis and binding) into quantifiable chemical or physical signals. Owing to its advantages of high specificity, high sensitivity, and rapid response, it is widely applied in fields including disease diagnosis, food safety, and environmental monitoring. This section introduces the applications of aptamers and DNAzymes in clinical pathogen detection, categorized by optical[74,158–167] and electrochemical[143,168–172] signals.

4.1. Optical biosensors

4.1.1. Colorimetric sensing. A key advantage of colorimetric biosensors is the ability to directly observe colour changes by the naked eye, without reliance on complex or sophisticated instrumentation, thereby lowering the operational barrier for detection. For norovirus (NoV), a global pathogen responsible for viral gastroenteritis, Bansal's group[158] developed a nanozyme–aptamer colorimetric sensor by integrating the NoV-specific AG3 aptamer with the peroxidase-mimicking activity of gold nanoparticles (GNPs). When the aptamer adsorbs onto the GNP surface, it suppresses the catalytic activity of the nanoparticles. In the presence of murine norovirus (MNV), the aptamer binds specifically to the virus and detaches from the GNPs, restoring their catalytic capability. This process enables oxidation of the colorless TMB substrate into a blue product (Fig. 7A). The sensor provides rapid detection within 10 min and exhibits ultrahigh sensitivity, with a calculated LOD of 30 virions per mL and an experimentally validated LOD of 200 virions per mL. It also maintains stable performance in human serum and shellfish homogenates, as well as under non-target microbial interference, with recovery rates ranging from 96.7–101.8%.

Similarly, Yang's group[159] leveraged the synergistic effects of DNA aptamer-mediated specific recognition and the peroxidase-mimetic activity of nanozymes to construct a multifunctional colorimetric platform based on Apt–CuSi@Fe, a hierarchical magnetic Fe_3O_4 nanozyme conjugate functionalized with copper silicate and *Enterococcus faecalis* (*E. faecalis*) aptamers. This platform enables selective capture, visual detection, and targeted killing of *E. faecalis*, and has been validated using oral-related samples, including *in vitro* bacterial suspensions and simulated root canal specimens. Notably, *E. faecalis* is the primary pathogen associated with secondary periapical periodontitis and can cause severe dental damage, such as root canal reinfection, abscess formation, and tooth loss, due to its strong biofilm-forming ability and antibiotic resistance. With a limit of detection of 2174 CFU mL^{-1}, bactericidal efficiency exceeding 98% at 50 μg mL^{-1}, a 66.94% biofilm inhibition rate, and good biocompatibility, this all-in-one system provides a practical tool for the precision management of *E. faecalis*-associated oral infectious diseases.

In another study, Li's group obtained a highly specific aptamer (RFD-SA6) targeting *Staphylococcus aureus* through *in vitro* selection.[74] Subsequent truncation and optimization yielded RFD-SA6T1, a 67-nucleotide variant that retains target-dependent catalytic activity in nasal mucus and exhibits no cross-reactivity with other bacteria. This aptamer was further integrated into a lateral flow device (LFD) (Fig. 7B). Using the DNAzyme-cleaved product as a bridging strand, the device mediates binding of DNA-modified GNPs to the test line, thereby generating a colorimetric signal. The LFD requires minimal sample pretreatment, enables detection of *S. aureus* in nasal mucus within 30 min, and achieves an LOD of 10^5 cells per mL. In addition, it can be stored for up to 6 months under dry, room-temperature conditions, outperforming commercial kits in stability and usability. This work provides a paradigm for detecting pathogenic bacteria in complex biological matrices.

4.1.2. Fluorescence sensing. Fluorescent biosensors couple biorecognition elements with fluorescent reporter moieties (*e.g.*, fluorophores, fluorescent dyes, fluorescent proteins, and quantum dots). When the biorecognition element interacts specifically with the target, it triggers changes in parameters of the fluorescent reporter—such as fluorescence intensity, wavelength, lifetime, or polarization. Target analysis is accomplished by detecting these signal changes.

Chen's group designed a multivalent aptamer probe (Multi-VAP) for diagnosis of pathogen *Salmonella*

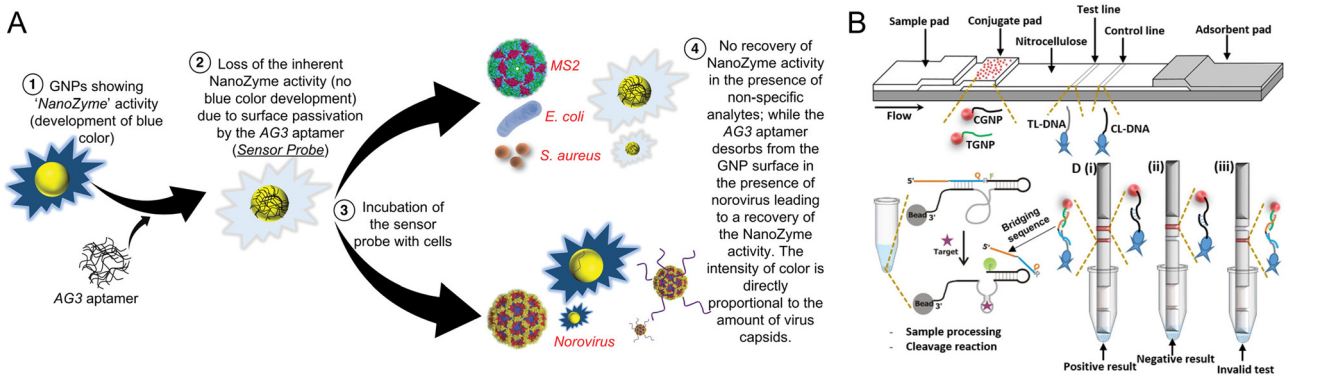

Fig. 7 (A) Schematic illustration of the aptamer-based nanozyme biosensor for norovirus detection. Reprinted with permission from ref. 158. Copyright 2019 American Chemical Society. (B) Design of a DNAzyme-based lateral flow device (LFD) for detection of *Staphylococcus aureus*. Reprinted with permission from ref. 74. Copyright 2022 Wiley-VCH Verlag GmbH & Co. KGaA, Weinheim.

infections.[160] Four aptamers were assembled *via* streptavidin, and dual Förster resonance energy transfer (FRET) effects, both intra- and inter-strand, were employed to suppress background fluorescence. In the presence of *Salmonella*, specific binding between the bacterium and the aptamers induces a conformational change in Multi-VAP, which subsequently initiates trigger-induced isothermal circular amplification (TICA). After a four-stage signal amplification process, "conformational change-induced fluorescence release, primer extension to increase fluorophore separation, cyclic aptamer recognition, and endonuclease-mediated cleavage for complete decoupling", detection is achieved within 30 min, with an LOD of 9 CFU mL^{-1} (Fig. 8A). Spike recovery rates in human serum samples ranged from 93.4% to 98.2%, and no cross-reactivity was observed with non-target bacteria, demonstrating a favourable balance between rapid detection and anti-interference capability in complex biological matrices.

To meet the demands for on-site detection of *S. aureus*, Lee's group[161] developed a smartphone-based fluorescent magnetic nanoparticle (FMNP) system. Aptamers were conjugated to FMNPs to construct integrated "recognition–labeling–enrichment" probes. Using the magnetic capture function of a dedicated detection cartridge, target enrichment was completed within 10 min. A fluorescence imaging module was built around a smartphone, employing a white

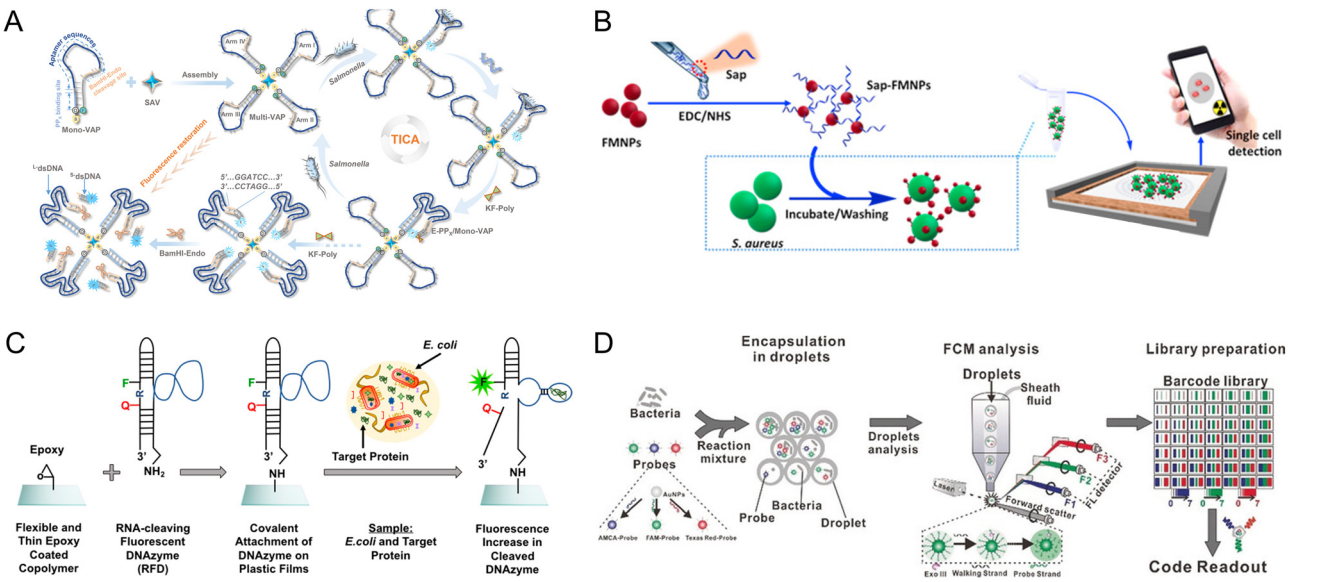

Fig. 8 (A) Schematic illustration of *Salmonella* detection using the multivalent aptamer probe (Multi-VAP) with trigger-induced isothermal rolling circle amplification (RCA). Reprinted with permission from ref. 160. Copyright 2022 American Chemical Society. (B) Schematic illustration of the aptamer-based fluorescent magnetic nanoparticle (FMNP) biosensor for *Staphylococcus aureus* detection. Reprinted with permission from ref. 161. Copyright 2018 Elsevier B.V. (C) DNAzyme-based cyclic olefin polymer (COP) film biosensor for *Escherichia coli* detection. Reprinted with permission from ref. 162. Copyright 2018 American Chemical Society. (D) Aptamer-mediated droplet microfluidic–stochastic DNA walker (SDwalker-Drop) platform for multiplex bacterial detection. Reprinted with permission from ref. 164. Copyright 2019 Wiley-VCH Verlag GmbH & Co. KGaA, Weinheim.

LED as the excitation source and utilizing filters to isolate specific fluorescent signals; quantitative analysis was performed by counting fluorescent spots (Fig. 8B). The system achieved an LOD of 10 CFU mL^{-1}, demonstrated good consistency in the detection of *S. aureus* from different sources (a fluorescence intensity variation of less than 10%), and fulfilled the requirements for portability and rapid response in point-of-care testing.

For *E. coli*, a common clinical pathogen, detection strategies need to be adapted to the non-invasive testing requirements in clinical practice. Didar's group[162] covalently immobilized *E. coli*-specific RFD-EC1 on a cyclic olefin polymer (COP) film. Fluorescent signal generation occurred *via* RNA cleavage, producing a transparent, flexible sensor that is well-suited for on-site clinical detection applications (Fig. 8C). This system enabled real-time monitoring of *E. coli* in clinical samples without complex sample pretreatment procedures. The sensor remained stable for over 14 days at pH 3–9, with an LOD of 10^3 CFU mL^{-1}, addressing a critical need for real-time detection in clinical testing workflows.

In a further optimization of this platform to mitigate component interference from complex clinical biological samples (*e.g.*, non-specific adsorption and fluorescent signal disturbances), Didar's group[163] embedded the *E. coli*-specific RFD-EC1 into a lubricant-infused surface (LIS) to fabricate an LISzyme sensor. By combining the RNA-cleavage-based fluorescent signaling of RFDs with the anti-biofouling properties of LIS, the latter can reduce component interference from complex clinical biological samples such as proteins and riboflavin. This optimized sensor can complete the *E. coli* detection within 1 h with an LOD of 250 CFU mL^{-1} and exhibits applicability to various clinical samples.

Given that different fluorophores exhibit distinct absorption and emission properties, multiplex fluorescent biosensors for pathogens can be constructed. Pei's group[164] developed a droplet microfluidic–stochastic DNA walker (SDwalker-Drop) platform. GNPs modified with thiol groups served as 3D tracks, loaded with three fluorescently labeled probe strands (AMCA-, FAM-, and TR-labeled). In the presence of targets, aptamer–target binding releases walker strands. Catalyzed by Exo III, the walker strands move autonomously along the tracks and gradually cleave the probe strands, releasing fluorophores from the quenching effect of gold nanoparticles to generate fluorescent signals. Simultaneously, the system encapsulates multicolor SDwalkers in water-in-oil-in-water (W/O/W) double emulsion droplets (Fig. 8D). Two-dimensional barcodes (based on color and intensity) were constructed by adjusting the type and intensity of fluorophores, achieving a theoretical coding capacity of $8^3 - 1 = 511$ and practical recognition of 20 pathogenic bacterial combinations. The platform had an LOD of 1 CFU mL^{-1}, stable signal readout after 4 h of incubation, and compatibility with clinical samples (*e.g.*, human serum and urine). When coupled with flow cytometry, the detection throughput reached several kilohertz, effectively overcoming the bottlenecks of multiplexing and high throughput in traditional fluorescence detection.

4.1.3. Surface-enhanced Raman spectroscopy (SERS) sensing. SERS leverages the electromagnetic and chemical enhancement effects of metal nanostructures to convert molecular vibration signals into light signals of specific wavelengths *via* Raman scattering. Combining high sensitivity and specificity, it serves as a critical technique for trace substance detection—an advantage particularly prominent in viral detection scenarios. Recently, Choo's group[165] developed a "signal-on/off" detection mechanism using Au nanopopcorn structures as SERS substrates (these structures form high-density "hotspots" to amplify signals) and aptamers with high affinity for the SARS-CoV-2 S protein. Prior to detection, Cy3 (labeled at the aptamer terminus) generates a strong signal due to its proximity to the substrate. In the presence of the SARS-CoV-2 target, aptamers preferentially bind to the S protein in viral lysates and detach from the substrate along with the target, causing a reduction in the Cy3 signal (Fig. 9A). Quantitative viral detection is achieved by monitoring this signal change. To improve detection reproducibility, 4-mercaptobenzoic acid (4-MBA) was used as an internal standard, reducing the relative standard deviation (RSD) of detection results to 2.3%. This method exhibited an LOD of 0.53 PFU mL^{-1}, with an LOD of 3.67 PFU mL^{-1} in clinically simulated samples containing nasopharyngeal swabs from negative patients. Detection was completed within 15 min, and its sensitivity was two orders of magnitude higher than that of commercial immunoassay kits. No cross-reactivity with influenza viruses was observed, fully demonstrating the application value of SERS in rapid and accurate viral detection.

4.1.4. Surface plasmon resonance (SPR) sensing. SPR exploits the plasmon resonance phenomenon of free electrons on metal film surfaces excited by specific incident light, converting changes in the refractive index of the metal surface (caused by molecular adsorption/binding) into optical signals such as resonance angle and light intensity. It enables real-time monitoring of intermolecular interactions without the need for labeling. In recent years, aptamer-based SPR biosensors have shown significant advantages in the rapid detection of pathogens. For example, two studies constructed highly specific and sensitive detection systems for *Klebsiella pneumoniae* (*K. pneumoniae*)[166] (causing urinary tract infections) and *Helicobacter pylori* (*H. pylori*)[167] (causing gastrointestinal infections), respectively.

For *K. pneumoniae* detection, Pattader's group[166] used AuNPs as localized SPR (LSPR) signal carriers. Aptamers specific to *K. pneumoniae* were modified on the AuNP surface *via* thiol (–SH) mediation to form Apt–AuNP complexes. Prior to detection, Apt–AuNPs formed chain-like structures driven by aptamer interactions, causing a slight red shift of the UV-vis absorption peak from ~525 nm (pure AuNPs) to ~528 nm. In the presence of *K. pneumoniae*, aptamers bound to bacterial surface receptors *via* specific three-dimensional conformations, guiding the aggregation of Apt–AuNPs on the

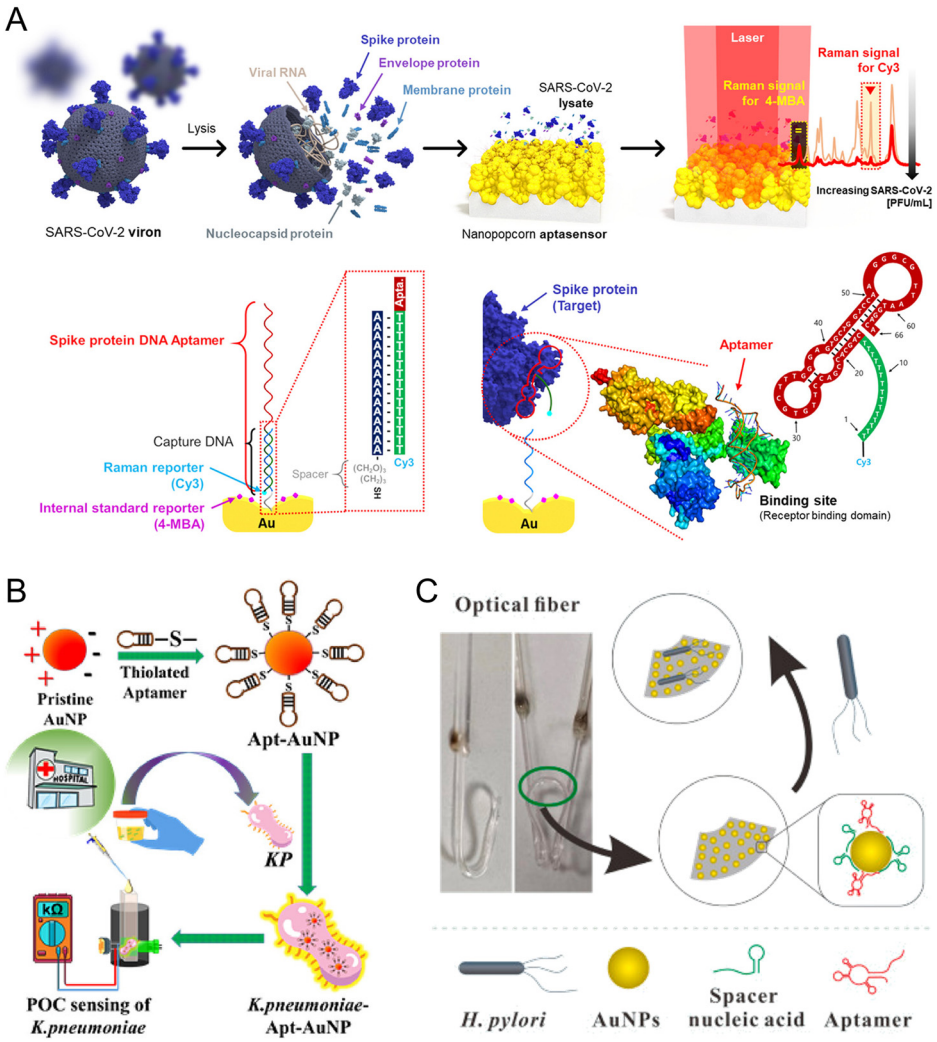

Fig. 9 (A) Schematic illustration of the aptamer-based Au nanopopcorn biosensor for SARS-CoV-2 detection. Reprinted with permission from ref. 165. Copyright 2021 American Chemical Society. (B) Schematic illustration of the aptamer-based gold nanoparticle biosensor for *Klebsiella pneumoniae* detection. Reprinted with permission from ref. 166. Copyright 2023 American Chemical Society. (C) Schematic illustration of the aptamer-based gold nanoparticle biosensor for *Helicobacter pylori* detection. Reprinted with permission from ref. 167. Copyright 2023 Elsevier B.V.

bacterial surface and triggering a hyperchromic effect in the LSPR signal (absorbance at 528 nm increased with bacterial concentration) (Fig. 9B). This sensor achieved an LOD of 3.4 × 10^3 CFU mL^{-1} and completed detection within 5 min, with no response to non-target bacteria (*e.g.*, *E. coli* and *S. aureus*). Additionally, a low-cost POC prototype built based on an LED–LDR (single-test cost ~$0.10) could be directly applied to clinical urine sample detection.

For *H. pylori* detection, Luo's group[167] used a J-type optical fiber probe as the substrate. Truncated and optimized *H. pylori*-specific aptamers, along with spacer nucleic acids (to regulate aptamer density), were modified on AuNPs on the fiber surface. Binding of the target bacterium to the aptamer altered the refractive index around the probe, inducing changes in the LSPR signal (Fig. 9C). This system achieved an LOD of 45 CFU mL^{-1}, completed detection of real water samples within 30 min, and exhibited spike recovery rates of 91.0–110.0%. Both systems rely on AuNP-mediated LSPR signal changes to enable rapid and accurate clinical detection of pathogens.

4.2. Electrochemical biosensors

4.2.1. Voltammetric sensing. Voltammetric biosensors apply a specific potential to an electrode modified with a biorecognition element, converting biomolecular interactions into redox current signals. Characterized by high sensitivity and strong anti-interference capability, they are commonly used for detecting pathogen biomarkers. Li's group[168] developed an electrochemical biosensor based on e-RCDs for rapid, culture-free detection of *E. coli*. This sensor integrates three core components: e-RCDs, dual-channel electrochemical chips (e-DChips), and three-dimensional nanostructured electrodes (e-NanoChannels). After e-RCDs

specifically recognize target bacteria, they undergo self-cleavage and release DNA barcodes labeled with methylene blue (an electroactive marker). The release channel of e-DChips immobilizes e-RCDs (resulting in decreased current after cleavage), while the capture channel binds to the barcodes *via* complementary single-stranded DNA probes (leading to increased current after binding) (Fig. 10A). e-NanoChannels enhance detection sensitivity, and bacterial quantification is ultimately achieved by measuring current changes using square wave voltammetry (SWV). This technology exhibits an LOD of 10^3 CFU mL^{-1} for *E. coli* and completes detection in less than 1 h. Clinical testing of 41 urine samples showed 100% sensitivity and 78% specificity. It can be integrated with miniaturized modules to detect undiluted urine, making it suitable for POC testing in scenarios such as urinary tract infections.

For HPV detection, diagnosis of infection can be achieved by detecting HPV capsid proteins. Szunerits' group[143] developed an electrochemical aptasensor based on a glassy carbon electrode modified with porous reduced graphene oxide/molybdenum disulfide (prGO/MoS_2). The prGO/MoS_2 composite constructs an electrode interface with high specific surface area and high conductivity. RNA aptamers (Sc5-c3) targeting the HPV-16 L1 protein are covalently immobilized on the electrode surface *via* EDC/NHS-activated carboxyl-amine reactions. Using $[Fe(CN)_6]^{4-}$ as a redox probe, the conformational change induced by the binding of the L1 protein to the aptamer reduces electron transfer efficiency, resulting in a decrease in peak current density measured by differential pulse voltammetry (DPV) (Fig. 10B). This sensor achieves an LOD of 0.1 ng mL^{-1} (1.75 pM) and enables accurate detection of the HPV-16 L1 protein in human serum and saliva samples, providing a novel strategy for the sensitive detection of HPV infections.

Porcine epidemic diarrhea virus (PEDV) causes a highly contagious intestinal disease in pigs, resulting in substantial economic losses to the livestock and aquaculture industry. Recently, Li's group[169] developed an aptamer sensor based on DNA barcodes for PEDV detection. The principle is as follows: on a dual-electrode electrochemical chip (DEE-Chip), electroactive aptamers bind to the N protein of PEDV and subsequently release DNA barcodes. Driven by an electric field, these barcodes migrate to the detection electrode, and detection is achieved by measuring changes in redox signals on the electrode using SWV (Fig. 10C). The LOD of this sensor reaches 6 nM (0.37 μg mL^{-1}) in saliva samples. During clinical evaluation, testing of 12 pig saliva samples showed a diagnostic sensitivity of 83%, specificity of 100%, and agreement of 92%, with an analysis time of only 1 h. This sensor requires no target amplification or labeling, providing an efficient tool for on-site POCT of PEDV in livestock farms.

4.2.2. Potentiometric sensing. Potentiometric biosensors detect changes in interfacial charge distribution induced by the binding of a biorecognition element to a target analyte, converting biomolecular interactions into quantifiable potentiometric signals. They require no complex signal amplification, offer rapid responses, and are suitable for detecting pathogens—aligning with the needs of POC testing scenarios. Recently, Bandaru's group[170] developed an

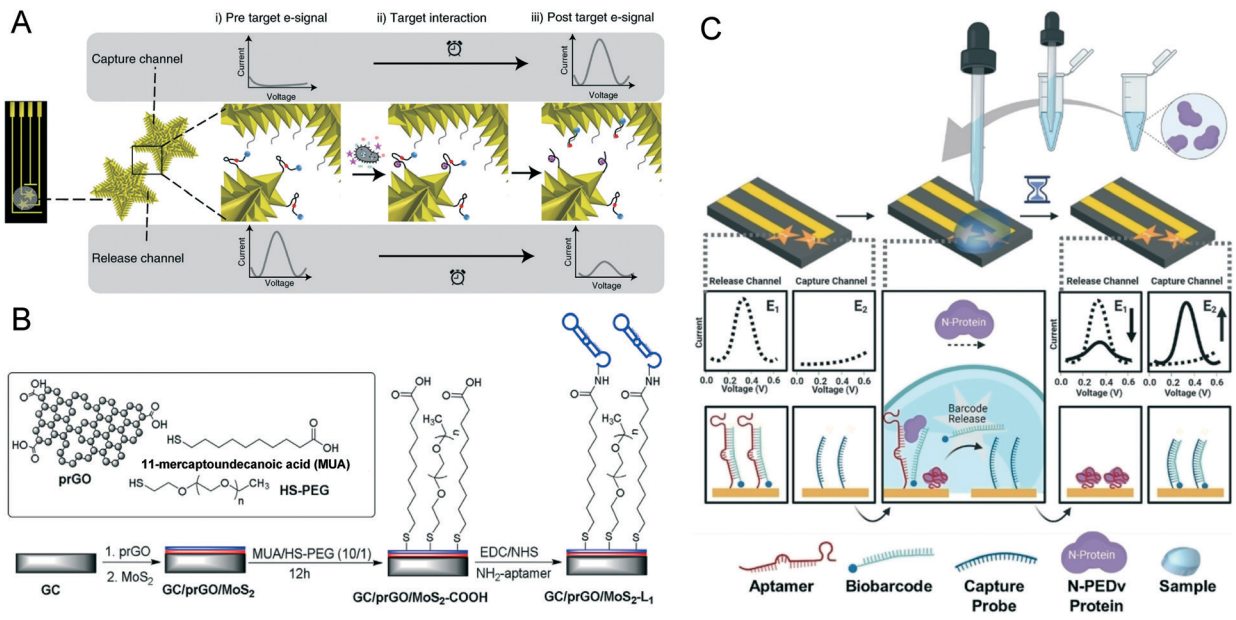

Fig. 10 (A) Schematic illustration of dual-channel signal changes induced by target-triggered e-RCD cleavage. Reprinted with permission from ref. 168. Copyright 2021 Springer Nature. (B) Schematic illustration of the aptamer-based prGO/MoS_2 composite electrode biosensor for human papillomavirus (HPV) detection. Reprinted with permission from ref. 143. Copyright 2018 Elsevier B.V. (C) Schematic illustration of the aptamer-based DEE-Chip dual-electrode biosensor for porcine epidemic diarrhea virus (PEDV) detection. Reprinted with permission from ref. 169. Copyright 2022 Wiley-VCH Verlag GmbH & Co. KGaA, Weinheim.

aptamer-conjugated graphene field-effect transistor (GFET) biosensor capable of detecting two types of unprocessed targets in saliva: intact SARS-CoV-2 viral particles (including the original strain and variants such as N501Y, D614G, and Omicron B1.1.529) and S protein, N protein, and S protein RBD. The principle involves covalently immobilizing aptamers targeting the S and N proteins on the GFET surface *via* 1-pyrenebutyric acid *N*-hydroxysuccinimide ester (PBASE). Binding of the target to the aptamers modulates the interfacial electric field, causing a change in the GFET's Dirac voltage (ΔV_D), which enables quantification (Fig. 11A). In terms of detection performance, for viral particles, the LOD was 1.28 PFU mL^{-1} for the S protein target and 1.45 PFU mL^{-1} for the N protein target, with detection completed within 20 min. The sensor exhibited a response of ≥40 mV to S/N/RBD proteins at concentrations ranging from fM to nM and could specifically distinguish between MERS-CoV and SARS-CoV-2. During the prevalence of the original SARS-CoV-2 strain, testing of 20 oral swab samples showed 100% positive percent agreement (PPA) and 100% negative percent agreement (NPA) with RT-PCR. During the Delta/Omicron prevalence period, testing of 26 saliva samples yielded a PPA of 66% and an NPA of 90%. The predicted positive rate was consistent with population epidemiological data, making the sensor suitable for POC testing and epidemiological surveillance.

4.2.3. Capacitive sensing. Capacitive biosensors use changes in the double-layer capacitance at the electrode interface as the core detection signal. They enable quantitative analysis of targets by altering the interfacial charge distribution or structure following the binding of a biorecognition element to the target analyte. Their key advantages include fast response speed, label-free detection, and low detection limits, making them suitable for rapid and accurate biomolecular detection.

Zika virus can be transmitted vertically from the mother to the fetus, causing microcephaly in fetuses. It can also spread through blood transfusion and sexual contact, and co-infection with dengue virus triggers acute tissue damage —posing a severe threat to public health. Recently, Lee's group[171] developed an aptamer-based capacitive biosensor for detecting ZIKV in human serum. The detection

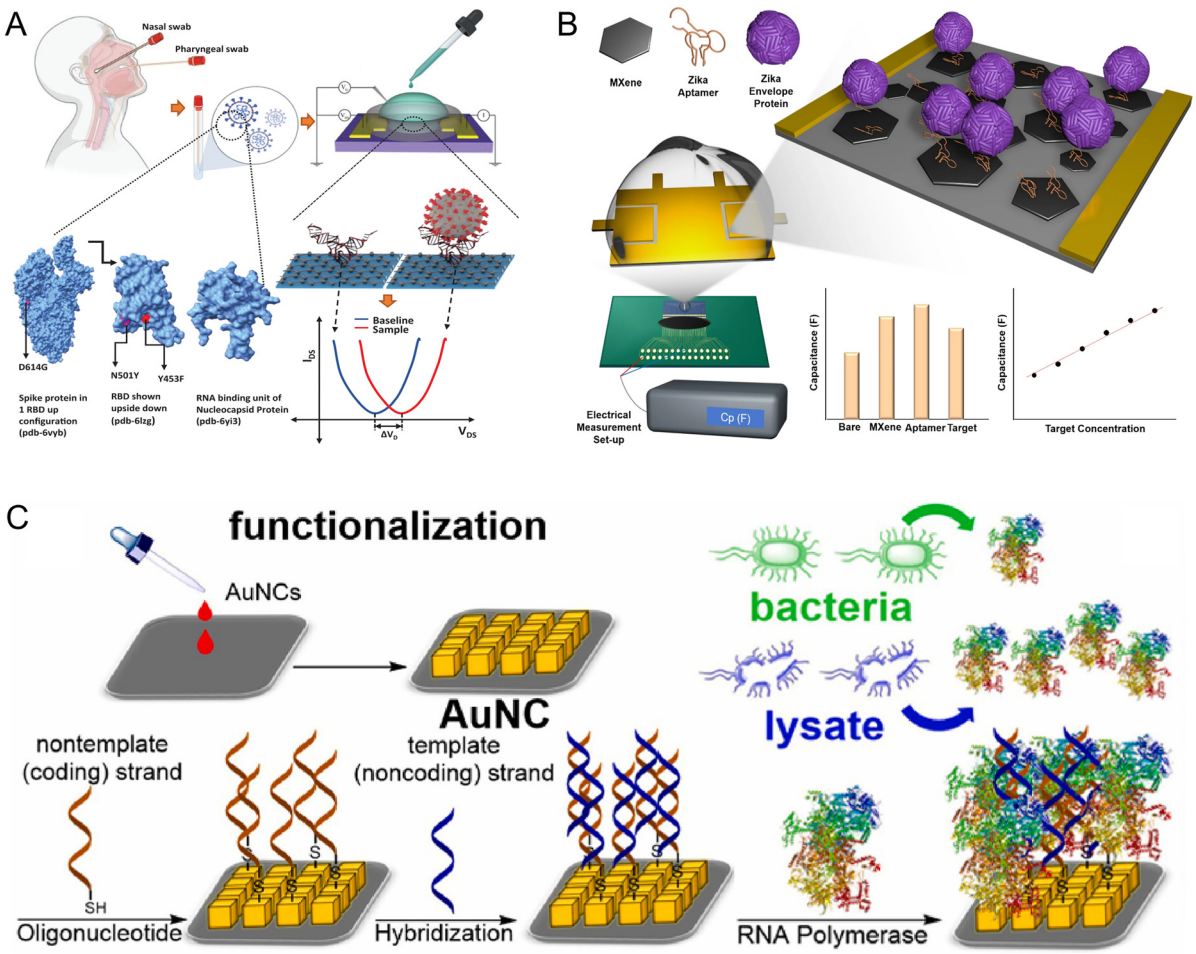

Fig. 11 (A) Schematic illustration of the aptamer-based graphene field-effect transistor (GFET) biosensor for SARS-CoV-2 detection. Reprinted with permission from ref. 170. Copyright 2022 National Academy of Sciences. (B) Schematic illustration of the aptamer-based MXene biosensor for Zika virus detection. Reprinted with permission from ref. 171. Copyright 2022 Springer Nature. (C) Schematic illustration of the aptamer-based AuNC/GCE biosensor for *Escherichia coli* detection. Reprinted with permission from ref. 172. Copyright 2023 Elsevier B.V.

principle is as follows: using gold microgap electrodes (AuMGEs)/printed circuit boards (PCBs) as the substrate, $Ti_3C_3T_X$ MXene (to enhance conductivity and reaction area) and aptamers targeting the ZIKV envelope protein are sequentially immobilized on the AuMGE surface, forming an aptamer/MXene heterolayer. When the Zika virus envelope protein in the sample specifically binds to the aptamers, it alters the dielectric properties of the electrode interface, leading to changes in capacitance signals. Quantification is achieved by detecting these capacitance changes at a frequency of 1 MHz using an inductance–capacitance–resistance (LCR) meter (Fig. 11B). This sensor exhibits a low LOD of 38.14 pM in 10% human serum samples and completes detection within 10 seconds. It shows no significant cross-reactivity with hemoglobin, bovine serum albumin, or dengue virus envelope protein, with a blind test error rate of ≤5.243%. It enables efficient and specific detection of ZIKV in human serum.

4.2.4. Impedimetric sensing. Impedimetric biosensors use changes in electrochemical impedance at the electrode interface as the core detection signal. They enable quantitative analysis of targets by altering the interfacial charge transfer or diffusion resistance following the binding of a biorecognition element to the target analyte. Their key advantages include label-free detection, simple operation, and broad target applicability, making them suitable for rapid detection of various biomarkers.

Uropathogenic *E. coli* (UPEC) is the primary pathogen causing hospital-acquired urinary tract infections (UTIs). It easily forms biofilms, which complicate treatment and pose a severe threat to public health. Recently, Ryl's group[172] developed an impedimetric biosensor based on multivariate impedance discriminant analysis (MIDA) for rapid detection of UPEC in human urine. The detection principle is as follows: using a planar glassy carbon electrode (GCE) as the substrate, aptamer-functionalized gold nanocubes (AuNCs) with self-assembly properties are drop-cast to form a sensing interface, where the aptamers target the RNA polymerase of *E. coli*. By real-time monitoring of multi-frequency impedance signals and combining singular value decomposition (SVD) with partial least squares-discriminant analysis (PLS-DA), "fingerprint signals" of macromolecular interactions can be extracted from raw impedance data without the need for an electrical equivalent circuit. When *E. coli* binds to the aptamers, the electrode interface impedance undergoes specific changes, which enables quantification (Fig. 11C). This sensor exhibits a low LOD of 11.3 CFU mL^{-1} for the UPEC-57 strain. At a negative overpotential of −0.35 to −0.10 V (*vs.* Ag/AgCl), its sensitivity and accuracy exceed 80%, with detection completed within 2 min. In clinical sample testing, it achieves specific recognition of UPEC in real human urine without the need for anti-contamination strategies, with a blind test error rate of ≤5.243%. This provides an efficient tool for the rapid diagnosis of urinary tract infections.

Different biosensor readouts exhibit strengths and limitations in sensitivity, portability, and clinical applicability, guiding the design of pathogen detection platforms. Colorimetric sensing is simple, label-free, and suitable for resource-limited POC settings but less sensitive. Fluorescence detection offers higher sensitivity and multiplexing potential, though it usually requires additional modifications. SERS and SPR provide real-time, label-free analysis with high sensitivity, but require specialized equipment and precise control. Electrochemical biosensors excel in sensitivity, miniaturization, and POC compatibility. Their performance depends on electrode quality and can be affected by electroactive species, and precise quantification still requires instrumentation.

In summary, optical readouts are preferable for visual detection, multiplexing, or real-time monitoring, whereas electrochemical readouts are better for high-sensitivity, miniaturized POC applications. Selection of biosensor readouts should be guided by the clinical context and performance requirements.

5. Current challenges and perspectives

FNAs offer advantages including high-specificity target recognition, programmable designability and facile conjugation with signal modules. These properties have enabled the rapid development of aptamer- and DNAzyme-based biosensors for detecting a wide range of pathogens. Importantly, FNA-based biosensors have been applied to clinical samples, such as serum, saliva, and urine, demonstrating their significant diagnostic potential.

Despite these advantages, FNAs still face challenges that limit their broader application. First, the development of functional nucleic acids (FNAs) relies heavily on the labor-intensive and time-consuming SELEX technique, which is inefficient, costly, associated with low success rates, and highly dependent on experimental experience. Second, low-abundance pathogen targets in clinical samples are difficult to detect, and high background signals can compromise detection accuracy. Third, conventional FNAs are typically composed of only the four canonical nucleotides (A, T, C, and G), which restricts their chemical functionality. Fourth, although FNAs are stable under optimized buffer conditions, nucleic acids are inherently susceptible to enzymatic degradation due to the widespread presence of nucleases in biological environments. In clinical samples, such as undiluted serum and saliva, FNAs can be inactivated through nuclease degradation and protein-mediated desorption, posing a barrier to effective clinical use.

To address these limitations and improve the performance of FNA-based biosensors, several strategies can be adopted. Artificial intelligence (AI)-assisted rational design has emerged as a powerful complement to traditional SELEX. By analyzing sequence–structure–activity relationships, predicting binding affinity, and modeling structural stability, AI and machine learning significantly shorten screening

cycles and reduce labor-intensive experimentation. Platforms such as RhoDesign[173] and UltraSelex[174] have successfully applied structure-to-sequence learning and computational ranking to design high-affinity aptamers. Innovations in screening methods, like the hydrogel-based HAS, further enhance enrichment efficiency and reduce nonspecific binding.[175] Despite these advances, AI predictions still require experimental verification, and most new screening methods target easily accessible molecules; applicability to complex targets remains to be explored. Overall, integrating AI with optimized experimental workflows offers a promising route to accelerate functional nucleic acid development for diagnostics and therapeutics.

The second strategy is careful design of selection libraries, which is aimed at obtaining high-affinity FNAs to address the challenge of low target abundance in clinical samples. By optimizing library conformations rather than relying solely on sequence randomness, the abundance of functional sequences can be increased, enhancing the likelihood of isolating high-affinity, high-specificity FNAs for pathogen targets and reducing the number of SELEX rounds required. For example, pre-structured libraries embed random target-binding regions within stable hairpin stems, pre-enriching aptamer-like molecules,[37] minimizing interference from constant regions, and simplifying secondary structure analysis and sequence optimization. For DNAzymes, new selection strategies are critical for identifying highly active DNAzymes. High-activity DNAzymes can be obtained by combining activity-driven selection pressures, rational library design, and kinetic screening. For example, instead of starting from a fully random library, embedding a known catalytic core into the initial library can efficiently and rapidly generate new and highly active DNAzymes.

The third strategy is chemical modification, which is used to address both the limited chemical functionality and the susceptibility to enzymatic degradation of FNAs. Modifications can be introduced either during selection of FNAs using chemically modified libraries or after selection. Traditional modifying targets of DNA include the phosphate backbone, sugar, or bases, but their synthesis, cost, and potential impact on PCR amplification during selection need to be assessed. In addition to improving stability against nuclease degradation, chemical modifications can also enhance FNA binding affinity or catalytic activity and expand their chemical functionality. For example, a recent chemoenzymatic method enables site-specific incorporation of functional groups into DNA,[176] markedly improving DNAzyme catalysis. A single carboxyl modification increased catalytic activity 100-fold, while dual carboxyl and benzyl modifications boosted activity nearly 700-fold, showing their potential for practical diagnostic applications.

In summary, overcoming the challenges of aptamer- and DNAzyme-based biosensors for pathogen detection requires targeted strategies to address limitations in development efficiency, target specificity, chemical functionality, and stability. Complementary approaches, including AI-assisted design, advances in screening methods, optimized library design, and chemical modification, help resolve the key bottlenecks that restrict the broader application of traditional FNAs.

Conflicts of interest

The authors declare no conflicts of interest.

Data availability

Not applicable as no data were used in producing this review article.

Acknowledgements

This work was supported by the National Key R&D Program (2024YFA0918900), the National Natural Science Foundation of China (NSFC 22476014, 22425602), and the Programme of Introducing Talents of Discipline to Universities (B25041).

References

1 E. Cesewski and B. N. Johnson, *Biosens. Bioelectron.*, 2020, **159**, 112214.
2 A. A. Patil, P. Kaushik, R. D. Jain and P. P. Dandekar, *ACS Infect. Dis.*, 2023, **9**, 9–22.
3 D. J. D. Earn, J. Ma, H. Poinar, J. Dushoff and B. M. Bolker, *Proc. Natl. Acad. Sci. U. S. A.*, 2020, **117**, 27703–27711.
4 L. Spinney, *Nature*, 2020, **584**, 30–32.
5 M. J. Dorman, D. Domman, T. Poklepovich, C. Tolley, G. Zolezzi, L. Kane, M. R. Viñas, M. Panagópulo, M. Moroni, N. Binsztein, M. I. Caffer, S. Clare, G. Dougan, G. P. C. Salmond, J. Parkhill, J. Campos and N. R. Thomson, *Nat. Commun.*, 2020, **11**, 4918.
6 B. Gilbertson and K. Subbarao, *Annu. Rev. Virol.*, 2023, **10**, 25–47.
7 R. D. Simkin, B. A. Han, V. C. Radeloff, S. LaDeau, F. Schug and K. C. Seto, *Global Change Biol.*, 2025, **31**, e70039.
8 R. Wang, Y. Han, R. Zhang, J. Zhu, X. Nan, Y. Liu, Z. Yang, B. Zhou, J. Yu, Z. Lin, J. Li, P. Chen, Y. Wang, Y. Li, D. Liu, X. Shi, X. Wang, Q. Zhang, Y. R. Yang, T. Li and L. Zhang, *Immunity*, 2023, **56**, 2635–2649.
9 F. Meng, H. Yang, Z. Qu, Y. Chen, Y. Zhang, Y. Zhang, L. Liu, X. Zeng, C. Li, Y. Kawaoka and H. Chen, *Proc. Natl. Acad. Sci. U. S. A.*, 2022, **119**, e2203919119.
10 L. R. Wong, J. Zheng, A. Sariol, S. Lowery, D. K. Meyerholz, T. Gallagher and S. Perlman, *Proc. Natl. Acad. Sci. U. S. A.*, 2021, **118**, e2102983118.
11 C. Adaken, J. T. Scott, R. Sharma, R. Gopal, S. Dicks, S. Niazi, S. Ijaz, T. Edwards, C. C. Smith, C. P. Cole, P. Kamara, O. Kargbo, H. A. Doughty, J. van Griensven, P. W. Horby, S. M. Gevao, F. Sahr, R. J. Dimelow, R. S. Tedder, M. G. Semple, W. A. Paxton and G. Pollakis, *Nature*, 2021, **590**, 468–472.
12 P. V'Kovski, A. Kratzel, S. Steiner, H. Stalder and V. Thiel, *Nat. Rev. Microbiol.*, 2021, **19**, 155–170.

13 S. G. Yedire, H. Khan, T. AbdelFatah, R. S. Moakhar and S. Mahshid, *Sens. Diagn.*, 2023, **2**, 763–780.
14 S. Mishra, P. R. Singh, X. Hu, L. Lopez-Quezada, A. Jinich, R. Jahn, L. Geurts, N. Shen, M. A. DeJesus, T. Hartman, K. Rhee, M. Zimmerman, V. Dartois, R. M. Jones, X. Jiang, R. Almada-Monter, L. Bourouiba and C. Nathan, *Proc. Natl. Acad. Sci. U. S. A.*, 2025, **122**, e2425981122.
15 G. Y. C. Cheung, J. S. Bae and M. Otto, *Virulence*, 2021, **12**, 547–569.
16 S. F. Khan, P. Rathod, V. K. Gupta, P. B. Khedekar and R. V. Chikhale, *Anal. Chem.*, 2024, **96**, 8124–8146.
17 J. E. Schmitz, C. W. Stratton, D. H. Persing and Y. W. Tang, *J. Clin. Microbiol.*, 2022, **60**, e0244621.
18 N. P. G. Gauthier, S. D. Chorlton, M. Krajden and A. R. Manges, *Clin. Microbiol. Rev.*, 2023, **36**, e0011922.
19 I. Martínez-Baz, A. Miqueleiz, N. Egüés, I. Casado, C. Burgui, A. Echeverría, A. Navascués, M. Fernández-Huerta, M. G. Cenoz and C. Trobajo-Sanmartín, *J. Infect. Public Health*, 2023, **16**, 410–417.
20 B. R. McConn, A. L. Kraft, L. M. Durso, A. M. Ibekwe, J. G. Frye, J. E. Wells, E. M. Tobey, S. Ritchie, C. F. Williams, K. L. Cook and M. Sharma, *Sci. Total Environ.*, 2024, **927**, 172190.
21 B. S. Alford, C. M. Hughes, D. F. Gilpin and J. W. McGrath, *J. Hosp. Infect.*, 2025, **164**, 8–17.
22 T. Dong, G. Sun, Z. Yang, Y. Jiao, J. Li, Z. Lin, X. Zhang, Z. Bian and A. Liu, *Chem. Eng. J.*, 2024, **497**, 154826.
23 Y. Peng, Y. Huang, F. Kiessling, D. Renn and M. Rueping, *ACS Synth. Biol.*, 2025, **14**, 420–430.
24 Y.-H. Liu, H. Zhang, K.-K. Yu, X.-F. Pei, J.-N. Xu, S.-Y. Chen, X.-Q. Yu and K. Li, *Sens. Diagn.*, 2024, **3**, 822–826.
25 L. Anjos, A. Z. Loukissas and D. M. Power, *Methods Mol. Biol.*, 2022, **2498**, 397–411.
26 D. Kodama, M. Tanaka, T. Matsuzaki, S. Nozuma, E. Matsuura, H. Takashima, S. Izumo and R. Kubota, *J. Clin. Microbiol.*, 2021, **59**, e03230.
27 C. D. Martin, A. T. Bender, B. P. Sullivan, L. Lillis, D. S. Boyle and J. D. Posner, *Sens. Diagn.*, 2024, **3**, 421–430.
28 W. R. de Araujo, H. Lukas, M. D. T. Torres, W. Gao and C. de la Fuente-Nunez, *ACS Nano*, 2024, **18**, 1757–1777.
29 N. Soxpollard, S. Strauss, R. Jungmann and I. S. MacPherson, *Commun. Chem.*, 2024, **7**, 174.
30 H. Boyd and A. F. Santos, *J. Allergy Clin. Immunol.*, 2025, **155**, 275–285.
31 N. Le Bert and T. Samandari, *Cell. Mol. Immunol.*, 2024, **21**, 159–170.
32 C. Tuerk and L. Gold, *Science*, 1990, **249**, 505–510.
33 A. D. Ellington and J. W. Szostak, *Nature*, 1990, **346**, 818–822.
34 R. R. Breaker and G. F. Joyce, *Chem. Biol.*, 1994, **1**, 223–229.
35 E. M. McConnell, I. Cozma, Q. Mou, J. D. Brennan, Y. Lu and Y. Li, *Chem. Soc. Rev.*, 2021, **50**, 8954–8994.
36 Y. Ding and J. Liu, *Anal. Chem.*, 2023, **95**, 14651–14658.
37 J. Li, Z. Zhang, J. Gu, H. D. Stacey, J. C. Ang, A. Capretta, C. D. M. Filipe, K. L. Mossman, C. Balion, B. J. Salena, D. Yamamura, L. Soleymani, M. S. Miller, J. D. Brennan and Y. Li, *Nucleic Acids Res.*, 2021, **49**, 7267–7279.
38 N. Lin, L. Wu, X. Xu, Q. Wu, Y. Wang, H. Shen, Y. Song, H. Wang, Z. Zhu, D. Kang and C. Yang, *ACS Appl. Mater. Interfaces*, 2021, **13**, 9306–9315.
39 J. Zhou and J. Rossi, *Nat. Rev. Drug Discovery*, 2017, **16**, 181–202.
40 S. Stangherlin, N. Lui, J. H. Lee and J. Liu, *TrAC, Trends Anal. Chem.*, 2025, 118349.
41 K. Y. Wong, M. S. Wong, J. H. Lee and J. Liu, *Adv. Drug Delivery Rev.*, 2025, **224**, 115646.
42 Y. Zhao, X. Zuo, Q. Li, F. Chen, Y.-R. Chen, J. Deng, D. Han, C. Hao, F. Huang and Y. Huang, *Sci. China: Chem.*, 2021, **64**, 171–203.
43 Z. Zhang, B. R. Adhikari, P. Sen, L. Soleymani and Y. Li, *Adv. Agrochem*, 2023, **2**, 246–257.
44 R. Liu, J. Li, B. J. Salena and Y. Li, *Angew. Chem., Int. Ed.*, 2025, **64**, e202418725.
45 D. Chang, S. Zakaria, S. Esmaeili Samani, Y. Chang, C. D. M. Filipe, L. Soleymani, J. D. Brennan, M. Liu and Y. Li, *Acc. Chem. Res.*, 2021, **54**, 3540–3549.
46 L. Zhu, J. Ling, Z. Zhu, T. Tian, Y. Song and C. Yang, *Anal. Bioanal. Chem.*, 2021, **413**, 4563–4579.
47 Z. Zhang, P. Sen, B. R. Adhikari, Y. Li and L. Soleymani, *Angew. Chem., Int. Ed.*, 2022, **61**, e202212496.
48 J. Li, Z. Zhang, R. Liu, R. Amini, B. J. Salena and Y. Li, *TrAC, Trends Anal. Chem.*, 2023, **158**, 116886.
49 P. J. Huang and J. Liu, *ChemistryOpen*, 2020, **9**, 1046–1059.
50 S. Qian, D. Chang, S. He and Y. Li, *Anal. Chim. Acta*, 2022, **1196**, 339511.
51 M. He, Z. Wang, X. Wu, Z. Du, C. Cui, Z. Zhao, Y. Sun, X. B. Zhang, L. He and W. Tan, *Angew. Chem., Int. Ed.*, 2025, **64**, e202424687.
52 R. D. Dunphy, P. Lasserre, L. Riordan, K. R. Duncan, C. McCormick, P. Murray and D. K. Corrigan, *Sens. Diagn.*, 2022, **1**, 841–850.
53 S. Muniandy, K. L. Thong, J. N. Appaturi, C. W. Lai and B. F. Leo, *Sens. Diagn.*, 2022, **1**, 1209–1217.
54 A. S. Paparella, B. L. Aboulache, R. K. Harijan, K. S. Potts, P. C. Tyler and V. L. Schramm, *Nat. Commun.*, 2021, **12**, 6285.
55 S. Agarwal-Jans, *Cell*, 2020, **183**, 550.
56 Y. Liu, Z. Chao, W. Ding, T. Fang, X. Gu, M. Xue, W. Wang, R. Han and W. Sun, *Cell. Mol. Biol. Lett.*, 2024, **29**, 34.
57 A. G. Shaw, T. K. Mampuela, E. L. Lofiko, C. Pratt, C. Troman, E. Bujaki, Á. O'Toole, J. O. Akello, A. A. Aziza, E. K. Lusamaki, J. C. Makangara, M. Akonga, Y. Lay, B. Nsunda, B. White, D. Jorgensen, E. Pukuta, Y. Riziki, K. E. Rankin, A. Rambaut, S. Ahuka-Mundeke, J. J. Muyembe, J. Martin, N. C. Grassly and P. Mbala-Kingebeni, *Nat. Microbiol.*, 2023, **8**, 1634–1640.
58 H. Xu, J. Sun, H. Wang, Y. Zhang and X. Sun, *Food Chem.*, 2021, **365**, 130409.
59 S. Syed, A. Rahaman, A. Mondal, S. Shaligram and S. P. Pawar, *Sens. Diagn.*, 2024, **3**, 354–380.
60 U. Ornellas-Garcia, P. Cuervo and F. L. Ribeiro-Gomes, *Front. Immunol.*, 2023, **14**, 1122411.

61 J. A. Nweze, F. N. Mbaoji, Y. M. Li, L. Y. Yang, S. S. Huang, V. N. Chigor, E. A. Eze, L. X. Pan, T. Zhang and D. F. Yang, *Infect. Dis. Poverty*, 2021, **10**, 9.
62 K. Bamba, K. Takabe, H. Daitoku, Y. Tanaka, A. Ohtani, M. Ozawa, A. Fukamizu, N. Nomura, A. Kohara and T. Kunoh, *Sens. Diagn.*, 2024, **3**, 287–294.
63 A. Aguzzi, *Science*, 2024, **383**, eadn9424.
64 P. Hermann and I. Zerr, *Nat. Rev. Neurol.*, 2022, **18**, 363–376.
65 D. G. J. Larsson and C. F. Flach, *Nat. Rev. Microbiol.*, 2022, **20**, 257–269.
66 N. Pardi and D. Weissman, *Nat. Biomed. Eng.*, 2020, **4**, 1128–1133.
67 H. F. Florindo, R. Kleiner, D. Vaskovich-Koubi, R. C. Acúrcio, B. Carreira, E. Yeini, G. Tiram, Y. Liubomirski and R. Satchi-Fainaro, *Nat. Nanotechnol.*, 2020, **15**, 630–645.
68 C. Li, Z. Zhu, J. Yao, Z. Chen and Y. Huang, *Molecules*, 2024, **29**, 4891.
69 M. M. Ali, S. D. Aguirre, H. Lazim and Y. Li, *Angew. Chem.*, 2011, **123**, 3835–3838.
70 Z. Shen, Z. Wu, D. Chang, W. Zhang, K. Tram, C. Lee, P. Kim, B. J. Salena and Y. Li, *Angew. Chem.*, 2016, **128**, 2477–2480.
71 M. M. Ali, A. Slepenkin, E. Peterson and W. Zhao, *ChemBioChem*, 2019, **20**, 906–910.
72 M. M. Ali, M. Wolfe, K. Tram, J. Gu, C. D. M. Filipe, Y. Li and J. D. Brennan, *Angew. Chem., Int. Ed.*, 2019, **58**, 9907–9911.
73 M. Rothenbroker, E. M. McConnell, J. Gu, M. L. Urbanus, S. E. Samani, A. W. Ensminger, C. D. M. Filipe and Y. Li, *Angew. Chem., Int. Ed.*, 2021, **60**, 4782–4788.
74 M. M. Ali, R. Silva, D. White, S. Mohammadi, Y. Li, A. Capretta and J. D. Brennan, *Angew. Chem., Int. Ed.*, 2022, **61**, e202112346.
75 Q. Feng, S. Zakaria, D. Morrison, K. Tram, J. Gu, B. J. Salena and Y. Li, *Angew. Chem., Int. Ed.*, 2023, **62**, e202306272.
76 S. Qian, D. Chang, J. Gu, B. J. Salena and Y. Li, *Chemistry*, 2023, **29**, e202300240.
77 X. Li, Y. Chang, Y. Wu and M. Liu, *Chem. Sci.*, 2024, **15**, 2996–3002.
78 J. Li, S. Khan, J. Gu, C. D. M. Filipe, T. F. Didar and Y. Li, *Angew. Chem., Int. Ed.*, 2023, **62**, e202300828.
79 D. Chang, T. Chang, B. Salena and Y. Li, *ChemBioChem*, 2020, **21**, 464–468.
80 Q. Zhou, G. Zhang, Y. Wu, Q. Zhang, Y. Liu, Y. Chang and M. Liu, *J. Am. Chem. Soc.*, 2023, **145**, 21370–21377.
81 X. Li, Y. Chang, Y. Wu and M. Liu, *Chem. Sci.*, 2024, **15**, 2996–3002.
82 K. Kruger, P. J. Grabowski, A. J. Zaug, J. Sands, D. E. Gottschling and T. R. Cech, *Cell*, 1982, **31**, 147–157.
83 M. Chandra, A. Sachdeva and S. K. Silverman, *Nat. Chem. Biol.*, 2009, **5**, 718–720.
84 A. Flynn-Charlebois, Y. Wang, T. K. Prior, I. Rashid, K. A. Hoadley, R. L. Coppins, A. C. Wolf and S. K. Silverman, *J. Am. Chem. Soc.*, 2003, **125**, 2444–2454.
85 J. R. Lorsch and J. W. Szostak, *Nature*, 1994, **371**, 31–36.
86 N. Carmi, S. R. Balkhi and R. R. Breaker, *Proc. Natl. Acad. Sci. U. S. A.*, 1998, **95**, 2233–2237.
87 B. Cuenoud and J. W. Szostak, *Nature*, 1995, **375**, 611–614.
88 Y. Li and R. R. Breaker, *Proc. Natl. Acad. Sci. U. S. A.*, 1999, **96**, 2746–2751.
89 Y. Li, Y. Liu and R. R. Breaker, *Biochemistry*, 2000, **39**, 3106–3114.
90 C. Zhou, J. L. Avins, P. C. Klauser, B. M. Brandsen, Y. Lee and S. K. Silverman, *J. Am. Chem. Soc.*, 2016, **138**, 2106–2109.
91 P. Pradeepkumar, C. Hobartner, D. A. Baum and S. K. Silverman, *Angew. Chem., Int. Ed.*, 2008, **47**, 1753.
92 Y. Li and D. Sen, *Nat. Struct. Biol.*, 1996, **3**, 743–747.
93 J. Kosman and B. Juskowiak, *Adv. Biochem. Eng./Biotechnol.*, 2020, **170**, 59–84.
94 M. Liu, D. Chang and Y. Li, *Acc. Chem. Res.*, 2017, **50**, 2273–2283.
95 S. Sherrill-Mix, Y. Hwang, A. M. Roche, A. Glascock, S. R. Weiss, Y. Li, L. Haddad, P. Deraska, C. Monahan, A. Kromer, J. Graham-Wooten, L. J. Taylor, B. S. Abella, A. Ganguly, R. G. Collman, G. D. Van Duyne and F. D. Bushman, *Genome Biol.*, 2021, **22**, 169.
96 S. Kim and A. Misra, *Annu. Rev. Biomed. Eng.*, 2007, **9**, 289–320.
97 K. Yang, D. N. Schuder, A. K. Ngor and J. C. Chaput, *J. Am. Chem. Soc.*, 2022, **144**, 11685–11692.
98 C. He, C. Lin, G. Mo, B. Xi, A. A. Li, D. Huang, Y. Wan, F. Chen, Y. Liang, Q. Zuo, W. Xu, D. Feng, G. Zhang, L. Han, C. Ke, H. Du and L. Huang, *Biosens. Bioelectron.*, 2022, **198**, 113857.
99 K. Yang and J. C. Chaput, *J. Am. Chem. Soc.*, 2021, **143**, 8957–8961.
100 J. Gu, A. Mathai, C. Nurmi, D. White, G. Panesar, D. Yamamura, C. Balion, J. Gubbay, K. Mossman, A. Capretta, B. J. Salena, L. Soleymani, C. D. M. Filipe, J. D. Brennan and Y. Li, *Chemistry*, 2023, **29**, e202300075.
101 A. Mathai, J. Gu, C. Nurmi, J. D. Brennan and Y. Li, *Angew. Chem., Int. Ed.*, 2025, **64**, e202507973.
102 J. Liu, Z. Cao and Y. Lu, *Chem. Rev.*, 2009, **109**, 1948–1998.
103 Q. Hu, Z. Tong, A. Yalikong, L. P. Ge, Q. Shi, X. Du, P. Wang, X. Y. Liu, W. Zhan, X. Gao, D. Sun, T. Fu, D. Ye, C. Fan, J. Liu, Y. S. Zhong, Y. Z. Jiang and H. Gu, *Nat. Chem.*, 2024, **16**, 122–131.
104 A. Roth and R. R. Breaker, *Proc. Natl. Acad. Sci. U. S. A.*, 1998, **95**, 6027–6031.
105 Y. Shen, W. Chiuman, J. D. Brennan and Y. Li, *ChemBioChem*, 2006, **7**, 1343–1348.
106 P. Röthlisberger and M. Hollenstein, *Adv. Drug Delivery Rev.*, 2018, **134**, 3–21.
107 M. Blind and M. Blank, *Mol. Ther.–Nucleic Acids*, 2015, **4**, e223.
108 H. Yu, J. Zhu, G. Shen, Y. Deng, X. Geng and L. Wang, *Microchim. Acta*, 2023, **190**, 255.
109 A. Bouvier-Müller and F. Ducongé, *Adv. Drug Delivery Rev.*, 2018, **134**, 94–106.

110 W. Zhou, R. Saran and J. Liu, *Chem. Rev.*, 2017, **117**, 8272–8325.
111 U. A. Ochsner, E. Katilius and N. Janjic, *Diagn. Microbiol. Infect. Dis.*, 2013, **76**, 278–285.
112 Y. Huang, X. Chen, N. Duan, S. Wu, Z. Wang, X. Wei and Y. Wang, *Food Chem.*, 2015, **166**, 623–629.
113 H. Yu, O. Alkhamis, J. Canoura, Y. Liu and Y. Xiao, *Angew. Chem., Int. Ed.*, 2021, **60**, 16800–16823.
114 X. L. Tang, S. M. Wu, Y. Xie, N. Song, Q. Guan, C. Yuan, X. Zhou and X. L. Zhang, *J. Infect.*, 2016, **72**, 573–586.
115 X. Sun, Q. Pan, C. Yuan, Q. Wang, X. L. Tang, K. Ding, X. Zhou and X. L. Zhang, *J. Am. Chem. Soc.*, 2016, **138**, 11680–11689.
116 S. Stangherlin, T. Malloch, A. J. Clarke and J. Liu, *Angew. Chem., Int. Ed.*, 2025, **64**, e202510518.
117 J. Li, Z. Zhang, R. Amini and Y. Li, *ChemMedChem*, 2022, **17**, e202200166.
118 M. Wang, M. C. Hao, Y. Huangfu, K. Z. Yang, X. Q. Zhang, Y. Zhang, J. Chen and Z. L. Zhang, *ACS Pharmacol. Transl. Sci.*, 2024, **7**, 249–258.
119 Q. Wang, J. Li, Z. Zhang, R. Amini, A. Derdall, J. Gu, J. Xia, B. J. Salena, D. Yamamura, L. Soleymani and Y. Li, *Angew. Chem., Int. Ed.*, 2025, **64**, e202415226.
120 B. I. Escudero-Abarca, S. H. Suh, M. D. Moore, H. P. Dwivedi and L. A. Jaykus, *PLoS One*, 2014, **9**, e106805.
121 A. Giamberardino, M. Labib, E. M. Hassan, J. A. Tetro, S. Springthorpe, S. A. Sattar, M. V. Berezovski and M. C. DeRosa, *PLoS One*, 2013, **8**, e79087.
122 T. Lu, Q. Ma, W. Yan, Y. Wang, Y. Zhang, L. Zhao and H. Chen, *Talanta*, 2018, **176**, 214–220.
123 A. S. Peinetti, R. J. Lake, W. Cong, L. Cooper, Y. Wu, Y. Ma, G. T. Pawel, M. E. Toimil-Molares, C. Trautmann, L. Rong, B. Mariñas, O. Azzaroni and Y. Lu, *Sci. Adv.*, 2021, **7**, eabh2848.
124 I. Hmila, B. Marnissi, M. Kamali-Moghaddam and A. Ghram, *Microbiol. Spectrum*, 2023, **11**, e0208122.
125 V. T. Nguyen, H. B. Seo, B. C. Kim, S. K. Kim, C. S. Song and M. B. Gu, *Biosens. Bioelectron.*, 2016, **86**, 293–300.
126 W. Alshaer, H. Hillaireau and E. Fattal, *Adv. Drug Delivery Rev.*, 2018, **134**, 122–137.
127 B. Powell Gray, L. Kelly, D. P. Ahrens, A. P. Barry, C. Kratschmer, M. Levy and B. A. Sullenger, *Proc. Natl. Acad. Sci. U. S. A.*, 2018, **115**, 4761–4766.
128 P. Dua, S. Kang, H. S. Shin, S. Kim and D. K. Lee, *Nucleic Acid Ther.*, 2018, **28**, 262–271.
129 S. Ramlal, B. Mondal, P. S. Lavu, B. N. and J. Kingston, *Int. J. Food Microbiol.*, 2018, **265**, 74–83.
130 T. T. Nguyen, E. R. Kim and M. B. Gu, *Biosens. Bioelectron.*, 2022, **198**, 113835.
131 P. Dua, S. Ren, S. W. Lee, J. K. Kim, H. S. Shin, O. C. Jeong, S. Kim and D. K. Lee, *Mol. Cells*, 2016, **39**, 807–813.
132 N. Duan, S. Wu, X. Chen, Y. Huang, Y. Xia, X. Ma and Z. Wang, *J. Agric. Food Chem.*, 2013, **61**, 3229–3234.
133 F. S. Bitaraf, I. Rasooli and S. L. Mousavi Gargari, *Eur. J. Clin. Microbiol. Infect. Dis.*, 2016, **35**, 503–510.
134 A. T. Bayraç and S. I. Donmez, *Anal. Biochem.*, 2018, **556**, 91–98.
135 W. Yan, L. Gu, S. Liu, W. Ren, M. Lyu and S. Wang, *J. Fish Dis.*, 2018, **41**, 1821–1829.
136 Q. Lu, S. Zhang, Y. Ouyang, C. Zhang, M. Liu, Y. Zhang and L. Deng, *Talanta*, 2023, **252**, 123857.
137 L. Hu, L. Wang, W. Lu, J. Zhao, H. Zhang and W. Chen, *Int. J. Mol. Sci.*, 2017, **18**, 2002489.
138 M. Zandieh, K. Patel and J. Liu, *Langmuir*, 2022, **38**, 1915–1922.
139 M. Zandieh, X. Luo, Y. Zhao, C. Feng and J. Liu, *Angew. Chem., Int. Ed.*, 2024, **64**, e202421438.
140 V. Domenyuk, Z. Gatalica, R. Santhanam, X. Wei, A. Stark, P. Kennedy, B. Toussaint, S. Levenberg, J. Wang, N. Xiao, R. Greil, G. Rinnerthaler, S. P. Gampenrieder, A. B. Heimberger, D. A. Berry, A. Barker, J. Quackenbush, J. L. Marshall, G. Poste, J. L. Vacirca, G. A. Vidal, L. S. Schwartzberg, D. D. Halbert, A. Voss, D. Magee, M. R. Miglarese, M. Famulok, G. Mayer and D. Spetzler, *Nat. Commun.*, 2018, **9**, 1219.
141 L. Y. Hung, C. Y. Fu, C. H. Wang, Y. J. Chuang, Y. C. Tsai, Y. L. Lo, P. H. Hsu, H. Y. Chang, S. C. Shiesh, K. F. Hsu and G. B. Lee, *Biomicrofluidics*, 2018, **12**, 054108.
142 X. Li, C. Yin, Y. Wu, Z. Zhang, D. Jiang, D. Xiao, X. Fang and C. Zhou, *Biosens. Bioelectron.*, 2020, **147**, 111488.
143 F. Chekin, K. Bagga, P. Subramanian, R. Jijie, S. K. Singh, S. Kurungot, R. Boukherroub and S. Szunerits, *Sens. Actuators, B*, 2018, **262**, 991–1000.
144 K. H. Lee and H. Zeng, *Anal. Chem.*, 2017, **89**, 12743–12748.
145 Y. Cao, J. Wang, F. Jian, T. Xiao, W. Song, A. Yisimayi, W. Huang, Q. Li, P. Wang, R. An, J. Wang, Y. Wang, X. Niu, S. Yang, H. Liang, H. Sun, T. Li, Y. Yu, Q. Cui, S. Liu, X. Yang, S. Du, Z. Zhang, X. Hao, F. Shao, R. Jin, X. Wang, J. Xiao, Y. Wang and X. S. Xie, *Nature*, 2022, **602**, 657–663.
146 Y. Cai, J. Zhang, T. Xiao, C. L. Lavine, S. Rawson, H. Peng, H. Zhu, K. Anand, P. Tong and A. Gautam, *Science*, 2021, **373**, 642–648.
147 S. M.-C. Gobeil, K. Janowska, S. McDowell, K. Mansouri, R. Parks, V. Stalls, M. F. Kopp, K. Manne, D. Li and K. Wiehe, *Science*, 2021, **373**, eabi6226.
148 D. Cyranoski, *Nature*, 2021, **589**, 337–339.
149 J. Müller, B. Wulffen, B. Pötzsch and G. Mayer, *ChemBioChem*, 2007, **8**, 2223–2226.
150 K. M. Ahmad, Y. Xiao and H. T. Soh, *Nucleic Acids Res.*, 2012, **40**, 11777–11783.
151 Y. Chen, X. Zhao, H. Zhou, H. Zhu, S. Jiang and P. Wang, *Nat. Rev. Immunol.*, 2023, **23**, 189–199.
152 J. D. Allen and T. M. Ross, *Hum. Vaccines Immunother.*, 2018, **14**, 1840–1847.
153 N. Winder, S. Gohar and M. Muthana, *Viruses*, 2022, **14**, 2811.
154 Z. Zhang, R. Pandey, J. Li, J. Gu, D. White, H. D. Stacey, J. C. Ang, C. J. Steinberg, A. Capretta, C. D. M. Filipe, K. Mossman, C. Balion, M. S. Miller, B. J. Salena, D. Yamamura, L. Soleymani, J. D. Brennan and Y. Li, *Angew. Chem., Int. Ed.*, 2021, **60**, 24266–24274.

155 J. Li, Z. Zhang, J. Gu, R. Amini, A. G. Mansfield, J. Xia, D. White, H. D. Stacey, J. C. Ang, G. Panesar, A. Capretta, C. D. M. Filipe, K. Mossman, B. J. Salena, J. B. Gubbay, C. Balion, L. Soleymani, M. S. Miller, D. Yamamura, J. D. Brennan and Y. Li, *J. Am. Chem. Soc.*, 2022, **144**, 23465–23473.
156 M. Sun, S. Liu, T. Song, F. Chen, J. Zhang, J. A. Huang, S. Wan, Y. Lu, H. Chen, W. Tan, Y. Song and C. Yang, *J. Am. Chem. Soc.*, 2021, **143**, 21541–21548.
157 Y. Su, Q. Cao, Y. Zhang, J. Cheng, X. Zhou, K. Dong, W. Zhou, L. Zhu, C. Zhao and R. Bai, *Chem. Eng. J.*, 2025, **509**, 161497.
158 P. Weerathunge, R. Ramanathan, V. A. Torok, K. Hodgson, Y. Xu, R. Goodacre, B. K. Behera and V. Bansal, *Anal. Chem.*, 2019, **91**, 3270–3276.
159 X. Yang, Y. Hu, H. Zhou, N. Lu, M. Zhang and Z. Tang, *Chem. Eng. J.*, 2025, **511**, 161848.
160 J. Xu, X. Zhang, C. Yan, P. Qin, L. Yao, Q. Wang and W. Chen, *Anal. Chem.*, 2022, **94**, 1357–1364.
161 S. Shrivastava, W. I. Lee and N. E. Lee, *Biosens. Bioelectron.*, 2018, **109**, 90–97.
162 H. Yousefi, M. M. Ali, H. M. Su, C. D. M. Filipe and T. F. Didar, *ACS Nano*, 2018, **12**, 3287–3294.
163 H. Yousefi, S. E. Samani, S. Khan, A. Prasad, A. Shakeri, Y. Li, C. D. M. Filipe and T. F. Didar, *ACS Nano*, 2022, **16**, 29–37.
164 M. Xiao, K. Zou, L. Li, L. Wang, Y. Tian, C. Fan and H. Pei, *Angew. Chem., Int. Ed.*, 2019, **58**, 15448–15454.
165 H. Chen, S. G. Park, N. Choi, H. J. Kwon, T. Kang, M. K. Lee and J. Choo, *ACS Sens.*, 2021, **6**, 2378–2385.
166 A. Deb, M. Gogoi, T. K. Mandal, S. Sinha and P. S. G. Pattader, *ACS Appl. Bio Mater.*, 2023, **6**, 3309–3318.
167 W. Ning, S. Hu, C. Zhou, J. Luo, Y. Li, C. Zhang, Z. Luo and Y. Li, *Anal. Chim. Acta*, 2023, **1278**, 341733.
168 R. Pandey, D. Chang, M. Smieja, T. Hoare, Y. Li and L. Soleymani, *Nat. Chem.*, 2021, **13**, 895–901.
169 A. Victorious, Z. Zhang, D. Chang, R. Maclachlan, R. Pandey, J. Xia, J. Gu, T. Hoare, L. Soleymani and Y. Li, *Angew. Chem., Int. Ed.*, 2022, **61**, e202204252.
170 D. K. Ban, T. Bodily, A. G. Karkisaval, Y. Dong, S. Natani, A. Ramanathan, A. Ramil, S. Srivastava, P. Bandaru and G. Glinsky, *Proc. Natl. Acad. Sci. U. S. A.*, 2022, **119**, e2206521119.
171 G. Park, M. Lee, J. Kang, C. Park, J. Min and T. Lee, *Nano Convergence*, 2022, **9**, 41.
172 A. Koterwa, M. Pierpaoli, B. Nejman-Faleńczyk, S. Bloch, A. Zieliński, W. Adamus-Białek, Z. Jeleniewska, B. Trzaskowski, R. Bogdanowicz, G. Węgrzyn, P. Niedziałkowski and J. Ryl, *Biosens. Bioelectron.*, 2023, **238**, 115561.
173 F. Wong, D. He, A. Krishnan, L. Hong, A. Z. Wang, J. Wang, Z. Hu, S. Omori, A. Li, J. Rao, Q. Yu, W. Jin, T. Zhang, K. Ilia, J. X. Chen, S. Zheng, I. King, Y. Li and J. J. Collins, *Nat. Comput. Sci.*, 2024, **4**, 829–839.
174 Y. Zhang, Y. Jiang, D. Kuster, Q. Ye, W. Huang, S. Fürbacher, J. Zhang, P. Doll, W. Lin, S. Dong, H. Wang, Z. Tang, D. Ibberson, K. Wild, I. Sinning, A. A. Hyman and A. Jäschke, *Nat. Chem. Biol.*, 2025, **21**, 1118–1126.
175 N. K. Singh, Y. Wang, C. Wen, B. Davis, X. Wang, K. Lee and Y. Wang, *Nat. Biotechnol.*, 2024, **42**, 1224–1231.
176 Z. Zhang, W. Wei, S. Chen, J. Yang, D. Song, Y. Chen, Z. Zhao, J. Chen, F. Wang, J. Wang, Z. Li, Y. Liang and H. Yu, *J. Am. Chem. Soc.*, 2024, **146**, 7052–7062.